

PREPARATION AND CHARACTERIZATION OF
NANOPAPER FROM REGENERATED CELLULOSE



A Thesis Submitted in Partial Fulfillment of the Requirements
for the Degree of Master of Engineering in Chemical Engineering
Department of Chemical Engineering
FACULTY OF ENGINEERING
Chulalongkorn University
Academic Year 2020
Copyright of Chulalongkorn University

การเตรียมและการวิเคราะห์คุณลักษณะของกระดาษนาโนจากเซลลูโลสที่ทำให้เกิดใหม่



วิทยานิพนธ์นี้เป็นส่วนหนึ่งของการศึกษาตามหลักสูตรปริญญาวิศวกรรมศาสตรมหาบัณฑิต

สาขาวิชาวิศวกรรมเคมี ภาควิชาวิศวกรรมเคมี

คณะวิศวกรรมศาสตร์ จุฬาลงกรณ์มหาวิทยาลัย

ปีการศึกษา 2563

ลิขสิทธิ์ของจุฬาลงกรณ์มหาวิทยาลัย

Thesis Title	PREPARATION AND CHARACTERIZATION OF NANOPAPER FROM REGENERATED CELLULOSE
By	Miss Nattorn Paijit
Field of Study	Chemical Engineering
Thesis Advisor	Professor SARAWUT RIMDUSIT, Ph.D.
Thesis Co Advisor	Professor SANONG EKGASIT, Ph.D.

Accepted by the FACULTY OF ENGINEERING, Chulalongkorn University
in Partial Fulfillment of the Requirement for the Master of Engineering

..... Dean of the FACULTY OF
ENGINEERING
(Professor SUPOT TEACHAVORASINSKUN, D.Eng.)

THESIS COMMITTEE

..... Chairman
(Associate Professor SOORATHEP KHEAWHOM,
Ph.D.)

..... Thesis Advisor
(Professor SARAWUT RIMDUSIT, Ph.D.)

..... Thesis Co-Advisor
(Professor SANONG EKGASIT, Ph.D.)

..... Examiner
(Professor SIRIPORN DAMRONGSAKKUL, Ph.D.)

..... External Examiner
(Associate Professor Chanchira Jubslip, D.Eng.)

จุฬาลงกรณ์มหาวิทยาลัย
CHULALONGKORN UNIVERSITY

ณัฐกร ไพจิตร : การเตรียมและการวิเคราะห์คุณสมบัติของกระดาษนาโนจากเซลลูโลสที่ทำให้เกิดใหม่. (PREPARATION AND CHARACTERIZATION OF NANOPAPER FROM REGENERATED CELLULOSE) อ.ที่ปรึกษาหลัก : ศ. ดร.ศราวุธ ริมคูสิต, อ.ที่ปรึกษาร่วม : ศ. ดร.สนอง เอกสิทธิ์

งานวิจัยนี้พัฒนากระดาษนาโนจากเซลลูโลสที่ทำให้เกิดใหม่ด้วยวิธีการหล่อโดยใช้ตัวทำละลาย เซลลูโลสที่ทำให้เกิดใหม่สามารถเตรียมได้จากกระบวนการละลายเยื่อคาลิปต์สฟอกขาวด้วยกรดฟอสฟอริก 85% ที่อุณหภูมิ -20 องศาเซลเซียส จากนั้นเติมน้ำเพื่อดึงกรดออกจากเซลลูโลส โดยงานวิจัยนี้ศึกษาผลของระยะเวลาการเก็บเส้นใยหลังการละลายที่อุณหภูมิ -20 องศาเซลเซียส ที่มีต่อการละลายของเส้นใย ณ เวลา 0, 20, 40, 60 นาที, 1 และ 2 วัน เซลลูโลสที่ทำให้เกิดใหม่ถูกพิสูจน์ด้วยสเปกตรัมของเทคนิค ATR FT-IR และค่าความเป็นผลึก นอกจากนี้ยังพบว่าค่าความเป็นผลึกของเส้นใยเริ่มคงที่ที่เวลา 60 นาที ซึ่งบ่งบอกว่าเส้นใยสามารถละลายได้อย่างสมบูรณ์ที่เวลา 60 นาที จากนั้นเยื่อคาลิปต์สฟอกขาวและกระดาษนาโนที่ได้จากเซลลูโลสที่ทำให้เกิดใหม่ ณ เวลาต่างๆ ถูกนำไปวิเคราะห์หาปริมาณธาตุที่เหลือ ณ อุณหภูมิ 600 องศาเซลเซียส พบว่าปริมาณธาตุของเยื่อคาลิปต์สฟอกขาวและกระดาษนาโน ณ เวลา 0 นาที เป็น 13.6 และ 24.9 ตามลำดับ ปริมาณธาตุที่เพิ่มขึ้นหลังจากการละลายและทำให้เกิดใหม่ เป็นเหตุผลมาจากเกิดหมู่ฟอสเฟตบริเวณพื้นผิวของเส้นใย ซึ่งมีคุณสมบัติเป็นสารหน่วงไฟ ทำให้กระดาษนาโนที่ได้จากการละลายเส้นใยด้วยกรดฟอสฟอริกมีความสามารถในการทนไฟได้ดี และในด้านคุณสมบัติเชิงกลของกระดาษนาโนมีค่าคงที่ ณ เวลา 60 นาที เป็นต้นไป ซึ่งสอดคล้องกับการละลายอย่างสมบูรณ์ของเส้นใย ดังนั้นในงานวิจัยนี้จึงนำกระดาษนาโน ณ เวลา 60 นาที มาเติมอนุภาคซิงค์ออกไซด์นาโนและนำไปทดสอบค่าให้แสงผ่านช่วงความยาวคลื่นตั้งแต่ 300-400 นาโนเมตร พบว่าการเติมซิงค์ออกไซด์นาโนที่ปริมาณ 3 เปอร์เซ็นต์โดยน้ำหนัก มีค่า 0.46 เปอร์เซ็นต์ ซึ่งที่ประสิทธิภาพเท่านี้แสดงถึงศักยภาพในการนำไปใช้ป้องกันรังสียูวีสำหรับฟิล์มป้องกันรังสียูวีได้

จุฬาลงกรณ์มหาวิทยาลัย
CHULALONGKORN UNIVERSITY

สาขาวิชา วิศวกรรมเคมี
ปีการศึกษา 2563

ลายมือชื่อนิสิต

ลายมือชื่อ อ.ที่ปรึกษาหลัก

ลายมือชื่อ อ.ที่ปรึกษาร่วม

6170159421 : MAJOR CHEMICAL ENGINEERING

KEYWORD Cellulose nanopaper, Regenerated cellulose, UV-blocking film
D:

Nattorn Paijit : PREPARATION AND CHARACTERIZATION OF NANOPAPER FROM REGENERATED CELLULOSE. Advisor: Prof. SARAWUT RIMDUSIT, Ph.D. Co-advisor: Prof. SANONG EKGASIT, Ph.D.

Cellulose nanopapers (RCNP) were prepared from regenerated cellulose (RC) via the solvent casting method. RC was prepared by dissolution of bleached eucalyptus cellulose pulp (BEP) with 85% H_3PO_4 at $-20^\circ C$. Water was applied as anti-solvent in the regenerated process. Effects of storage time after dissolution on fiber solubility were investigated at 0, 20, 40, 60 min, 1, and 2 days. ATR FT-IR spectra and crystalline index proved that regenerated cellulose was obtained. The crystalline index of the fiber became stable at 60 min, indicating the fibers were completely dissolved at 60 min. The results from thermogravimetric analysis showed that after the main degradation process, the remained char residue at $600^\circ C$ was close to 13.6% or 24.9% for original BEP or RCNP-0 min, respectively. The formation of phosphate groups on fiber surface caused increasing in remained char residue, indicating the RCNP had flame resistance property. Mechanical properties of RCNP were constant at 60 min of storage time, corresponding to the complete dissolution of fiber. Lastly, RCNP-60 min was embedded with zinc oxide nanoparticles. The UV-vis transmittance spectra of ZnO/cellulose nanopaper were investigated under a wavelength range of 300-400 nm. It was found that the 3 %wt. ZnO/cellulose nanopaper had a UV transmission value equal to 0.46%, indicating the potential usage of the cellulose nanopaper filled ZnO nanoparticles for UV-blocking films.



Field of Study: Chemical Engineering

Student's Signature

Academic Year: 2020

.....
Advisor's Signature

Year:

.....
Co-advisor's Signature

.....

ACKNOWLEDGEMENTS

First of all, I would like to convey my gratitude to my academic advisor, Professor Dr. Sarawut Rimdusit and Professor. Dr. Sanong Ekgasit. Without his kind direction and proper guidance, this thesis would have been a little successful. In every phase of research, his supervision and guidance shaped this thesis to be completed perfectly. Besides my advisor, I would like to thank my fellow lab mates in the polymer engineering laboratory, Chulalongkorn University for the productive discussion, information sharing, and your encouragement. Last but not the least, special thanks to my family and friends who always support me and walk with me through the rough time. This thesis was funded by the National Nanotechnology Center (NANOTEC), NSTDA, Ministry of Science and Technology, Thailand.

Nattorn Paijit



TABLE OF CONTENTS

	Page
ABSTRACT (THAI)	iii
ABSTRACT (ENGLISH).....	iv
ACKNOWLEDGEMENTS	v
TABLE OF CONTENTS.....	vi
CHAPTER I INTRODUCTION.....	1
CHAPTER II THEORY	1
2.1 Sources of cellulose	1
2.2 Structure of cellulose	1
2.3 Types of nanocellulose	3
2.3.1 Cellulose nanofibrils.....	3
2.3.2 Cellulose nanocrystals	3
2.3.3 Bacterial nanocellulose.....	3
2.4 Pretreatment of cellulose fibers.....	4
2.4.1 Enzymatic pretreatment.....	4
2.4.2 Alkaline-acid pretreatment	5
2.4.3 Pretreatment by ionic liquids	5
2.5 Preparation of cellulose nanofibrils	5
2.5.1 High pressure homogenization	6
2.5.2 Microfluidization	6
2.5.3 Grinding.....	6

2.5.4 Cryocrushing.....	6
2.5.5 High intensity ultrasonication.....	7
2.5.6 Hybrid mechanical approach	7
2.6 Regenerated cellulose	7
2.7 Fabrication of Cellulose Nanopapers.....	9
2.8 Performance of Cellulose Nanopapers.....	10
2.8.1 Mechanical properties of cellulose nanopapers	10
2.8.2 Tunable optical properties of cellulose nanopapers.....	10
2.8.3 Thermal properties of cellulose nanopapers	11
2.8.4 Surface roughness and shape stability of cellulose nanopapers	11
2.9 Applications of Cellulose Nanopapers	11
2.9.1 Highly transparent and flexible cellulose nanopaper electronics.....	11
2.9.2 Nanopaper as an optical sensing platform.....	12
2.9.3 Cellulose nanopapers as a membrane for water purification	13
CHAPTER III LITERATURE REVIEWS.....	14
CHAPTER IV EXPERIMENTAL	25
4.1 Raw materials.....	25
4.2 Preparation of regenerated cellulose	25
4.3 Preparation of cellulose nanopaper	25
4.4 Characterization method	25
4.4.1 Optical microscopy (OM)	25
4.4.2 Fourier transform infrared (FT-IR) spectroscopy	25
4.4.3 X-ray diffraction (XRD).....	26
4.4.4 Thermogravimetric analysis (TGA)	26

4.4.5 Universal testing machine	26
4.4.6 UV-visible spectroscopy	26
4.5 Objectives	26
4.6 Scopes of research.....	26
4.7 Procedure of the study	27
CHAPTER V RESULTS AND DISCUSSION	28
5.1 Eucalyptus cellulose dissolution in H_3PO_4 aqueous solution at low temperature	28
5.2. Eucalyptus cellulose structure	29
5.3. Properties of cellulose nanopaper	31
5.4. Molecular comparison of regenerated cellulose nanopaper (RCNP) and nanocrystalline cellulose nanopaper (NCCNP).....	33
5.5. ZnO nanoparticles embeded on cellulose nanopaper	35
CHAPTER VI CONCLUSIONS	39
REFERENCES	40
VITA.....	45

CHAPTER I

INTRODUCTION

One of the most abundant sources of polysaccharide from nature is cellulose with an estimated yield of 7.5×10^{10} tons/year [1], essentially occurring in wall plant wood, e.g. hemp, cotton, and other plant biomass. At present, bio-based materials were of high interested in several plants due to the depletion of fossil fuel resources, deterioration of environment, and climate change. Cellulose is therefore one of the promising candidates to substitute fossil fuel resources as it is renewable, bio-compatible, and bio-degradable. For pulp and paper industry, cellulose fiber has been used as raw material for thousands of years. This cellulose fiber can be isolated to obtain cellulose nanofibrils (CNFs), which can be processed into cellulose nanopaper. The diameter of CNFs is approximately 100 nm or lower and their length is in the range of few microns, accordingly aspect ratio of CNFs is in a high level. Thus, CNFs can be used as the building blocks to construct highly robust material structures, due to their high mechanical strength, low thermal expansion coefficient, optical transparency, and low porosity. Especially, cellulose nanopaper in the form of films represents as a green material for many applications, for example, transistors, organic light emitting diodes (OLEDs), tissue engineering, food packaging, substrate for sensor, mille-feuille filter paper, etc [2].

The separation of CNFs from plant fibers can be done by various processes, for example, fibrillation by mechanical process, enzymatic hydrolysis followed by mechanical fibrillation, 2,2,6,6-tetramethylpiperidine-1-oxyl (TEMPO) oxidation followed by mechanical fibrillation, and pretreatment with acid [2]. Wood is the main starting material for cellulose commercial production. However, cellulose produced by using wood as a raw material has a high molecular weight, causing a dense intersection and intensive network. Thus, a partial hydrolysis process is required to achieve a full fibrillation, but this process can reduce the cellulose material functionalities [3]. Recently, cellulose fibrillation was developed by direct dissolving without hydrolysis processing in a cold H_2SO_4 aqueous solution at temperature of $-20^\circ C$ [4]. However, this process has a drawback of cellulose degradation, which is

catalyzed by the sulfate group, especially if the temperature is too high, so the obtained CNFs have limited thermal stability and applications.

In this study, eucalyptus cellulose was dissolved directly in a cold aqueous solution of H_3PO_4 at the temperature of -20°C . The regenerated cellulose was obtained and processed into nanopaper. The chemical structure, thermal stability, and mechanical properties of nanopaper were investigated and reported.



CHAPTER II

THEORY

2.1 Sources of cellulose

Cellulose is the most abundant resources of natural fibers. The estimation quantity of cellulose extraction is greater than 7.5×10^{10} tons per year [1]. It is obtained from various sources including wood, seed(cotton), bast (flax, hemp), cane (bamboo, bagasse), leaf (sisal), straw (rice, wheat), fruit(coir), tunicate, fungi, algae, mineral and bacteria [5] (as illustrated in Figure 2.1).

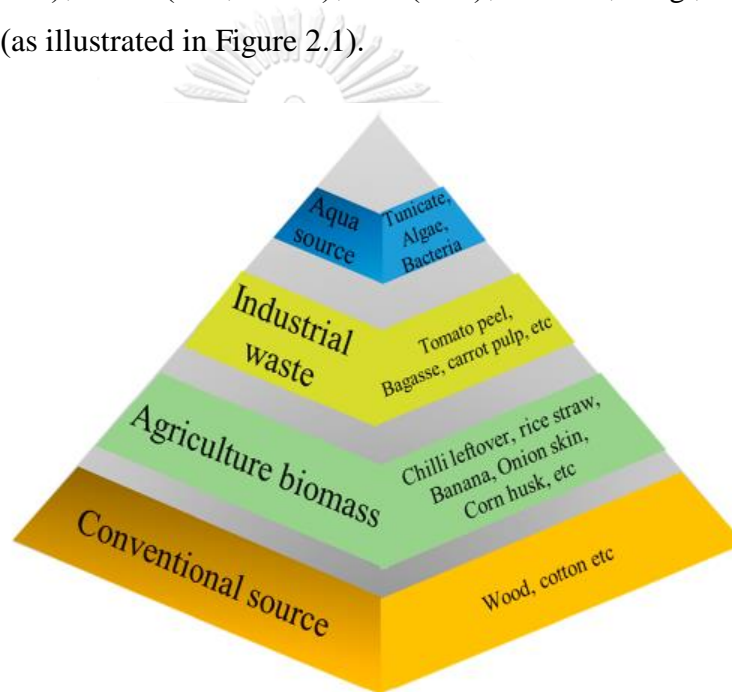


Figure 2.1 Hierarchical representation of various sources of cellulose [6].

2.2 Structure of cellulose

Cellulose appears as microfibrils in the plant cell wall of various sources. The fibril diameter varies in distinctive source [7]. Cellulose composes of a glucose monomer; β -1,4-linked anhydro-D-glucose (as illustrated in Figure 2.2). The cellulose polymerization degree is up to 20,000 units. Approximately, 10,000 units and 15,000 glucose units in wood and cotton respectively [8].

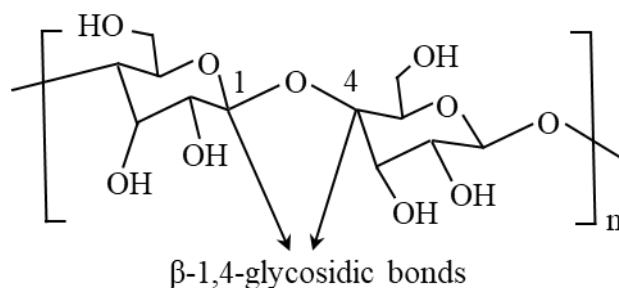


Figure 2.2 Chemical structure of cellulose.

The β-1,4-glycosidic bonds orderly build a crystalline structure by Van der Waals forces and intermolecular and intramolecular hydrogen bonding. In these regions, the cellulose chains are strongly arranged into crystallites. The hydrogen bonds exist between cellulose chains makes them extremely stable but poorly soluble in water and other solvents. Hydrogen bonding networks and molecular alignment result in cellulose polymorphs or allomorphs. There are six interconvertible polymorphs of cellulose that have been identified as cellulose I, II, III_I, III_{II}, IV_I, and IV_{II}. Generally, native cellulose has the crystal structure of cellulose I, which can be subdivided into allomorphs I_α and I_β [9, 10]. Cellulose I_α possesses a triclinic structure, whereas I_β has a monoclinic crystalline structure. Cellulose obtained from microbial and algal sources is rich in I_α. Cellulose, forming higher plant cell walls, is rich in I_β. The hydrogen bond breakdown and disorientation cause the amorphous region (as illustrated in Figure 2.3).

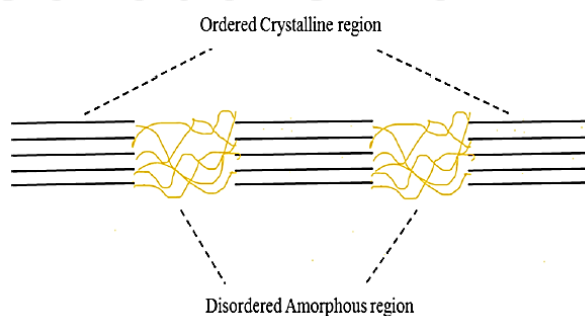


Figure 2.3 Crystalline and amorphous regions of cellulose .

2.3 Types of nanocellulose

The plant cell wall could be categorized into two parts; primary and secondary. The primary cell wall is the exterior layer; less than 1 μm , and the secondary cell wall mainly contains cellulose bundles. The hierarchical configurations of wood to cellulose nanocrystals (as illustrated in Figure 2.4). Each bundle consists of millions of microfibrils with 5-10 nm. All nanofiber is composed of flexible amorphous and strong crystalline parts.

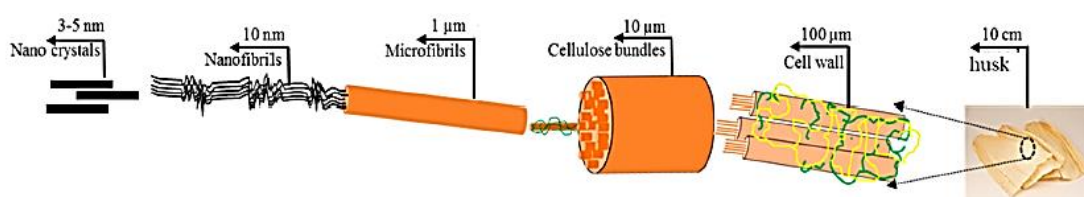


Figure 2.4 Hierarchical structure of cellulose and its derivatives in nanoscale .

2.3.1 Cellulose nanofibrils

CNFs are the smallest plant fiber structural unit. They are comprised of a bundle of extended cellulose chain molecules with flexible, long, and entangled nanofibers. They consist of alternating crystalline and amorphous domains. In general,

CNFs are produced by wood pulp delamination through mechanical pressure before and/or after chemical or enzymatic treatment [2].

2.3.2 Cellulose nanocrystals

On the contrary, cellulose nanocrystals (CNCs) have limited flexibility compared to CNFs because they do not contain amorphous regions. CNCs, also known as nanowhiskers, nanorods, and rod-like cellulose crystals, are commonly isolated from cellulose fibers through acid hydrolysis [2].

2.3.3 Bacterial nanocellulose

Bacterial nanocellulose (BNC) is synthesized by a bacterial family, referred to as *Gluconoacetobacter* (e.g., *Acetobacter xylinum*). These bacteria are able to convert glucose into cellulose materials. BNC is unlike the other two types of

nanocellulose in that it is formed by a bottom-up method in biotechnological processes [2].

2.4 Pretreatment of cellulose fibers

The plant cell wall is primarily made up of cellulose, lignin, and hemicellulose (as illustrated in Figure 2.5). Hemicellulose can be categorized into four different classes based on their structure: mannans, xylans, β -glucans, and xyloglucans. All four elements are branched polymer chain. Lignin is an irregular cross-linked polymer of heterogeneous phenyl propane, so it is used as binder. Xyloglucans are used as gelling agent in food. On the contrary, hemicellulose and lignin can hinder the fibrillation of cellulose which result in consuming higher amount of energy. This problem can be resolved with pretreatments including enzymatic, alkaline-acid pretreatment or pretreatment by ionic liquids [2].

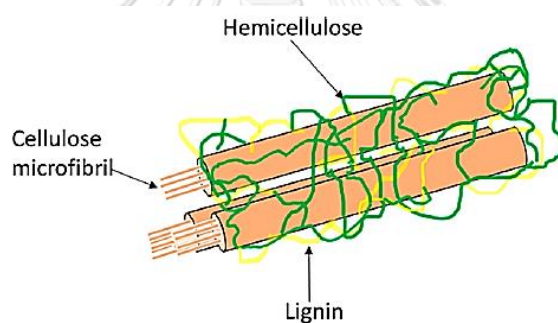


Figure 2.5 Cellulose bundles embedded by hemicelluloses and lignin [6].

2.4.1 Enzymatic pretreatment

Enzymes are selected to modify or degrade the lignin and hemicellulose contents while balancing the cellulose portion. On the other hand, enzymes encourage selective hydrolysis of a specified component or restrictive hydrolysis of several elements in the cellulosic fiber. Cellulose fibers contain distinctive organic compounds hence a single enzyme cannot decompose all the fibers. Cellulose enzymes can be classified into two groups. The first group includes cellobiohydrolases A and B-type cellulases which greatly attack the crystalline cellulose, and another group includes endoglucanases C and D-type cellulases which require the disordered structure in cellulose to attack. Numbers of investigations have been done

on the production of CNFs with enzymatic pretreatment. Mild enzymatic hydrolysis was combined with refining and homogenization to create CNFs from bleached softwood pulp [11]. Based on numbers of investigations have been done on the production of CNFs with enzymatic pretreatment found that the selective and mild hydrolysis using a single component endoglucanase enzyme allowed a better aspect ratio and was less aggressive compared to acid hydrolysis.

2.4.2 Alkaline-acid pretreatment

The alkaline-acid pretreatment was employed prior to mechanical isolation of CNFs for lignin, hemicellulose, and pectin solubilization. Commonly, the alkaline-acid pretreatment deals with three major steps. First, soaking fibers in 12-17.5 wt% NaOH solution for 2 hours to raise the cellulosic fiber surface area, and to make it more susceptible to hydrolysis. Then, hydrolyzing the fibers with 60-80°C hydrochloric acid solution to solubilize hemicelluloses. Following by treating the fibers with 2 wt% NaOH solution for 2 hours at 60-80°C. This last step would interrupt the lignin structure and break down the linkages between lignin and carbohydrate [12].

2.4.3 Pretreatment by ionic liquids

Ionic liquids are organic salts with a melting temperature below 100°C. They have unique and valuable properties such as nonflammability, chemical and thermal stability. Ionic liquids have been extensively used to dissolve cellulose materials such as 1-butyl-3-methylimidazolium chloride ($[Bmim]Cl$) and 1-ethyl-3-methylimidazolium acetate ($[C_2mim]OAc$) [13].

2.5 Preparation of cellulose nanofibrils

The CNF defibrillation requires intensive mechanical treatment. It is more productive to perform mechanical approach prior to the chemical pretreatment especially when cellulose came from the source with high molecular weight that causes dense intersection and network. Without appropriate mechanical approach, it can result to alter crystallinity, and crack cellulose hydrogen bonds. The reactivity of fibers Mechanical approaches to diminish cellulosic fibers into nanofibers can be

classified into homogenizing, microfluidization, grinding, cryocrushing, high intensity ultrasonication, and hybrid mechanical approach [2].

2.5.1 High pressure homogenization

High pressure homogenization process includes transferring the cellulose slurry under high pressure into a vessel via a very small nozzle. High pressure and velocity, as well as impact and shear forces on the fluid, generate shear rates in the stream and reduce the fiber size to the nanoscale. High pressure homogenization can be determined as an efficient method for refining cellulosic fibers because of its high efficiency, simplicity, and no organic solvents need. One of the most crucial things related to high pressure homogenization is the clogging issue because of its very small orifice size. In order to troubleshoot this drawback, it is required to reduce the size of the fibers before passing them through high pressure homogenization. Consequently, various mechanical pretreatments are used before high pressure homogenization [2].

2.5.2 Microfluidization

A microfluidizer is another equipment similar to high pressure homogenization which can be used to produce CNFs. A microfluidizer includes an intensifier pump to add the pressure and interaction chamber to defibrillate the fibers using shear and impact forces against colliding streams and channel walls [2].

2.5.3 Grinding

Another strategy to isolate cellulose into nano-size fibers is grinding. In grinding device, there is a static grindstone and a rotating grindstone and pulp slurry passes between these two stones. The fibrillation mechanism in the grinder is to shatter hydrogen bond and cell wall structure by shear forces and individualization of pulp to nanoscale fibers [2].

2.5.4 Cryocrushing

Cryocrushing is another technique for mechanical fibrillation of cellulose. In this procedure, water swollen cellulosic fibers are immersed in liquid nitrogen. Then, they are subsequently crushed using a mortar and pestle. Applied high impact force to the frozen cellulosic fibers, leads to cell wall rupture due to the exerted pressure by ice crystals and thus liberating nanofibers [2].

2.5.5 High intensity ultrasonication

High-intensity ultrasonication is a mechanical process in this methods we used oscillating power are applied to isolate CNFs by hydrodynamic forces of ultrasound [2].

2.5.6 Hybrid mechanical approach

Most mechanical methods relate to high energy consumption, which can cause a dramatic decrease in both yield and fibril length. These drawbacks can be overcome with the pretreatment of cellulose before mechanical fibrillation [2].

2.6 Regenerated cellulose

The natural form of cellulose, termed cellulose I or native cellulose, is obviously the most available form. Its three-dimensional structure is highly complex and may compose of two distinct crystalline forms, cellulose I_α and I_β. Cellulose I can be made to undergo an irreversible transition to a stable crystalline form, termed cellulose II, by chemical regeneration. The major supramolecular distinction of cellulose I (native) and cellulose II (re-crystallized) (as illustrated in Figure 2.6) [14]. Cellulose II can be produced by two different procedure including regeneration and mercerization. In general, the cellulose regeneration can be achieved from the dissolution of cellulose in organic non-solvents, ionic liquid, or acidic-containing aqueous solutions such as carbon disulfide, 1-butyl-3-methylimidazolium chloride ([Bmim]Cl), sulfuric acid etc [15]. Afterward, cellulose is regenerated by adding water. Therefore, these cellulose is known by the term “ regenerated cellulose” . Furthermore, regenerated cellulose can be made to the CNFs by mechanical fibrillation.

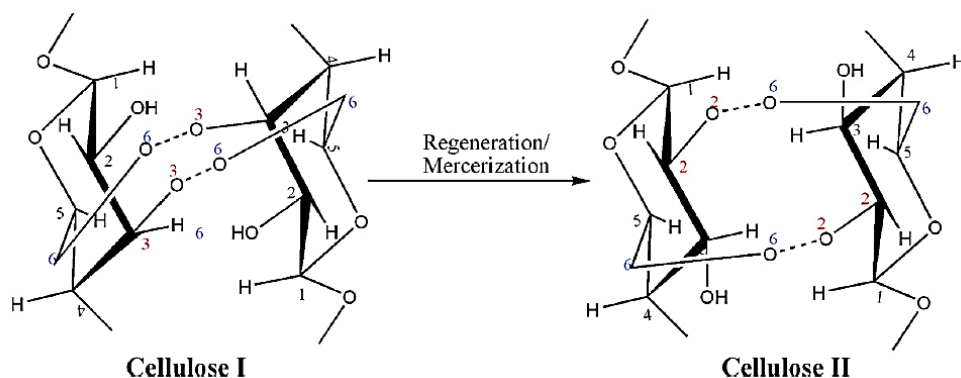


Figure 2.6 Conversion of the polymorphs of cellulose I to cellulose II [14].

A mechanism for the dissolution of cellulose in acidic-containing aqueous solutions. For the example, the dissolution of cellulose in a sulfuric acid aqueous solution. The sulfate ions and hydronium ions shape electron donor-acceptor complexes with the -OH groups in cellulose. As a result of the interactions between sulfuric acid and cellulose, the intra and intermolecular hydrogen bonds between hydroxyl groups in cellulose are broken down, leading to the separation of the molecular chains of cellulose (perceived as swelling) and extremely cellulose dissolution (as illustrated in Figure 2.7) [16].

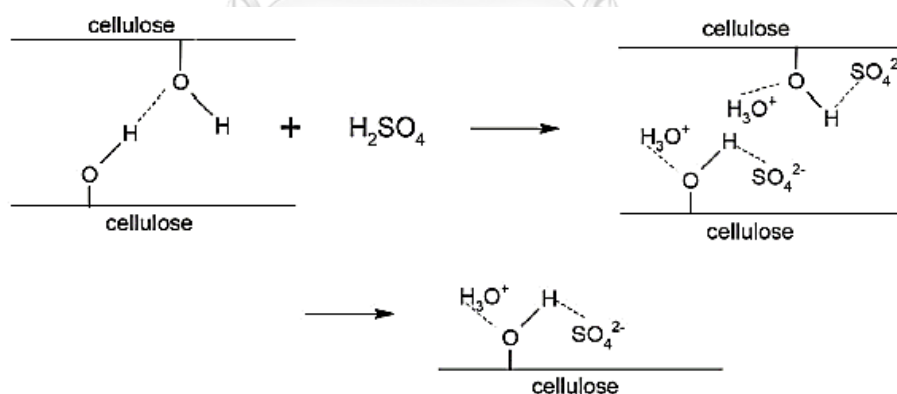


Figure 2.7 Dissolution mechanism of cellulose in sulfuric acid [16].

The cellulose dissolution mechanism in ionic liquids involves the oxygen and hydrogen atoms of cellulose-OH in the formation of electron donor-electron acceptor (EDA) complexes which interact with the ionic liquid (as illustrated in Figure 2.8). For their interaction, the cellulose atoms serve as electron pair donor and hydrogen atoms perform as an electron acceptor. In corresponding, the cations in ionic liquid

solvents act as the electron acceptor center and anion as electron-donor center. The two centers must be located close enough in space to allow the interactions and to allow the EDA complexes to form. Upon interaction of the cellulose-OH and the ionic liquid, the oxygen and hydrogen atoms from hydroxyl groups are separated, resulting hydrogen bond opening between molecular chains of the cellulose. Finally, the cellulose dissolved [17].

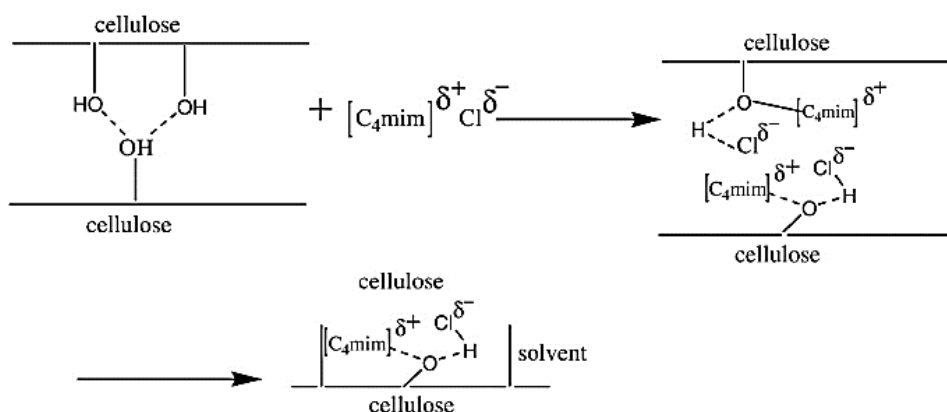


Figure 2.8 Dissolution mechanism of cellulose in ionic liquids [17].

2.7 Fabrication of Cellulose Nanopapers

Cellulose nanopapers can be explained as a network constructed by high aspect ratio (beyond 100), intertwined nanofibrils, and random orientation of surface nanofibrils. Nanopapers can be prepared by different approaches including pressure filtration, solvent casting, vacuum filtration, hot pressing and probably by drying the CNF suspension in a continuous rolling process. A schematic of cellulose nanopaper fabrication via filtration process (as illustrated in Figure 2.9) [18].

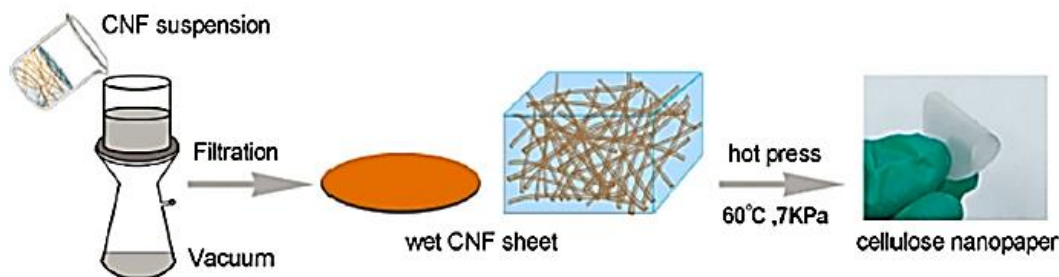


Figure 2.9 Fabrication of cellulose nanopaper via filtration process [18].

2.8 Performance of Cellulose Nanopapers

Cellulose nanopapers have many benefits both traditional paper and plastic in terms of optical transparency, surface roughness, mechanical properties, porosity, pore size, CTE, printability, and renewability, as shown in Table 2.1 [2].

Table 2.1 Comparison of Nanopaper, Traditional Paper and Plastic [2]

Characteristics	Nanopaper	Traditional Paper	Plastic
Surface Roughness (nm)	5	5,000-10,000	5
Porosity (%)	20-40	50	0
Pore Size (nm)	10-50	3,000	0
Optical Transparency at 550 nm (%)	90	20	90
Coefficient of Thermal Expansion (CTE) (ppm/K)	12-28.5	28-40	20-100
Max. Loading Stress (MPa)	200-400	6	50
Young's Modulus (GPa)	7.4-14	0.5	2-2.7
Printability	Good	Excellent	Poor

2.8.1 Mechanical properties of cellulose nanopapers

Cellulose nanopapers express the remarkably high tensile strength, Young's modulus, toughness, and strain to failure due to the tightly packed nanofibrillar network and numerous fiber-fiber hydrogen bonds. These properties manifest themselves as making nanopaper 10 times stronger than regular paper. Moreover, the tight packing of nanofibrils can be used to the food packaging due to high moisture and oxygen barrier properties [19].

2.8.2 Tunable optical properties of cellulose nanopapers

One of the interesting properties of cellulose nanopapers is their high optical transmittance and tunable optical haze. Traditional paper made from common fibers is opaque. However, the paper becomes transparent when the fibers go down to nanoscale due to denser structure. Most notably, light goes through the fibers without scattering when the fiber size and spacing are both much smaller than the wavelength of visible light. To result in, the nanopaper indicates high transparency. The light

scattering scales with the fiber diameter proportional to approximately D^3 , where D is the diameter of the fiber. Although the back light scattering is suppressed by the nanopaper surface, the individual nanofibers promote forward scattering, which causes the nanopaper indicates higher haze than plastic such as PET [2].

2.8.3 Thermal properties of cellulose nanopapers

The optically transparent nanopaper made of cellulose nanofibers has a CTE of <8.5 ppm/K, which is far lower than plastic (50 ppm/K). This is desirable since it can maintain the dimensional stability under thermal processing condition. Furthermore, Cellulose nanopapers can also tolerate a much higher processing temperature than plastic [2].

2.8.4 Surface roughness and shape stability of cellulose nanopapers

Electronics such as organic light emitting diodes, transistors, and radio frequency identification devices have a layered structure, and the thickness of the middle layer are commonly lower than 1 μm . The device have a significant leakage issue if the roughness of the substrate is at the micrometer scale. This is the challenge for electronics on regular paper. Whereas, Nanopapers made from CNFs with diameter 5-10 nm have critically low surface roughness due to the small fiber diameter. Thus, the low surface roughness of nanopapers can overcome this problem [2].

2.9 Applications of Cellulose Nanopapers

2.9.1 Highly transparent and flexible cellulose nanopaper electronics

Paper is an excellent choice to replace plastics as a substrate for flexible electronics due to its low cost, renewability, and flexibility. Cellulose nanopaper, a new type of paper which can produce from nano-sized cellulose fibers, is a promising substrate material for high transparent and flexible electronics (e.g. organic-light-emitting-diodes (OLED), transistors etc.) (as illustrated in Figure 2.10) due to its potentially high transparency, high mechanical strength and lightweight. Consequently, nanopaper can host many types of electronics that are not possible on traditional paper [3].

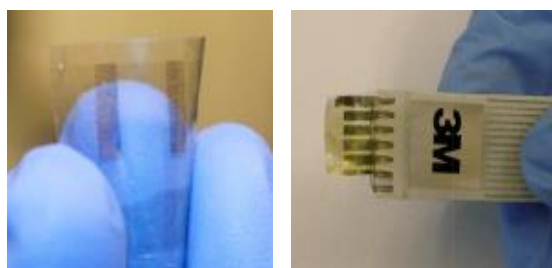


Figure 2.10 Highly transparent and flexible cellulose nanpaper transistor (left) and OLED (right).

2.9.2 Nanopaper as an optical sensing platform

Another vital area for nanopaper applications are sensors. Paper-based sensors promise to be simple, portable, disposable, low power-consuming, and inexpensive sensor devices. For the sample, a colorimetric-based sensor based on nanopaper containing embedded silver and gold nanoparticles, a photoluminescent-based sensor which can be photoexcited using UV-visible light, and a potential up-conversion sensing platform constructed from nanopaper functionalized with $\text{NaYF}_4:\text{Yb}^{3+}@\text{Er}^{3+}@\text{SiO}_2$ nanoparticles which can be photoexcited using infrared light (as illustrated in Figure 2.11) [20].

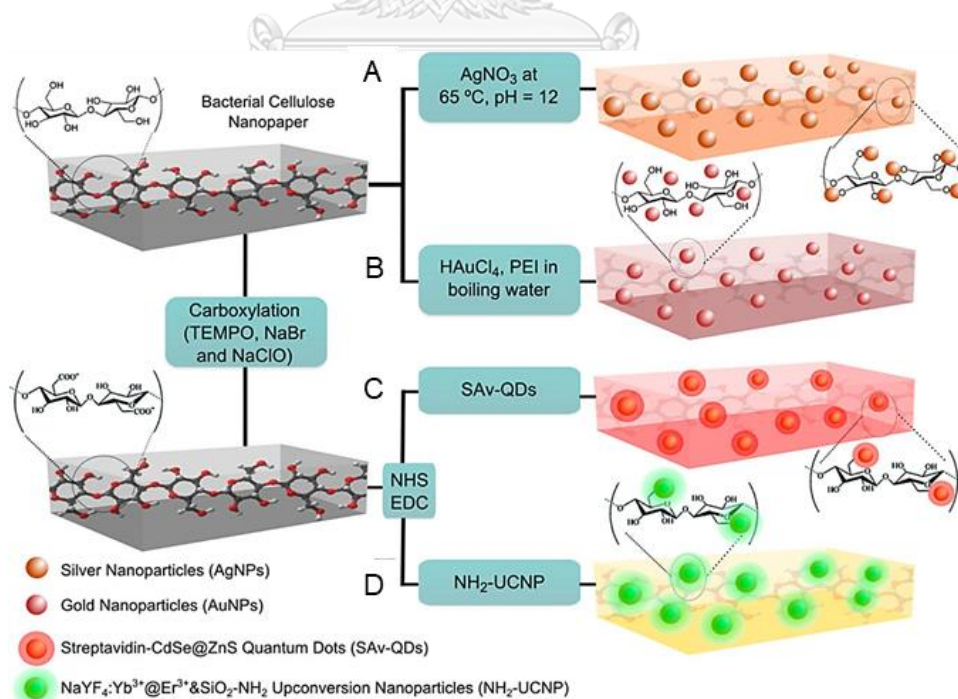


Figure 2.11 Schematic of the proposed nanopaper-based composites [20].

2.9.3 Cellulose nanopapers as a membrane for water purification

Another crucial area for nanopaper applications are sensors. Paper-based Membrane operations are important tools to lesson water contamination enabling supply of potable water for a growing number of people living on this planet. Conventional membranes for this task are commonly produced from synthetic polymers, derived from fossil resources or ceramics requiring great amounts of energy, chemicals, and solvents during their production. Furthermore, conventional filter papers produced from cellulose microfibrils, exhibit certain limitations when pollutants in the nanometer range are to be extracted. Therefore, utilization of membranes based on a renewable resource such as cellulose nanopapers could be an alternative [2].



CHAPTER III

LITERATURE REVIEWS

Malucelli *et al.* (2019) [21] investigated about effects of cellulose chemical pretreatment on energy consumption of produced cellulose nanofibers (CNFs) and mechanical properties of nanopaper. They produced CNF by chemically-modified bleached eucalyptus pulp (BEP) before defibrillation by using NaOH and TEMPO-mediated oxidation. It was found that the TEMPO-pretreatment greatly improved the mechanical properties of nanocellulose and presented as the most energy-efficient method. Fourier transform infrared spectroscopy (FTIR) and transmission electron microscopy (TEM) micrographs confirmed successful modification and defibrillation, respectively. Figure 3.1 presents the peak at 1730 cm^{-1} for the untreated pulp (BEP) that was attributed to the C=O stretching of hemicellulose. Whereas, this peak disappeared in BEP-NaOH and BEP-TEMPO. The absence of peaks in this region for BEP-NaOH and BEP-TEMPO suggested that hemicellulose was removed through the chemical pretreatment.

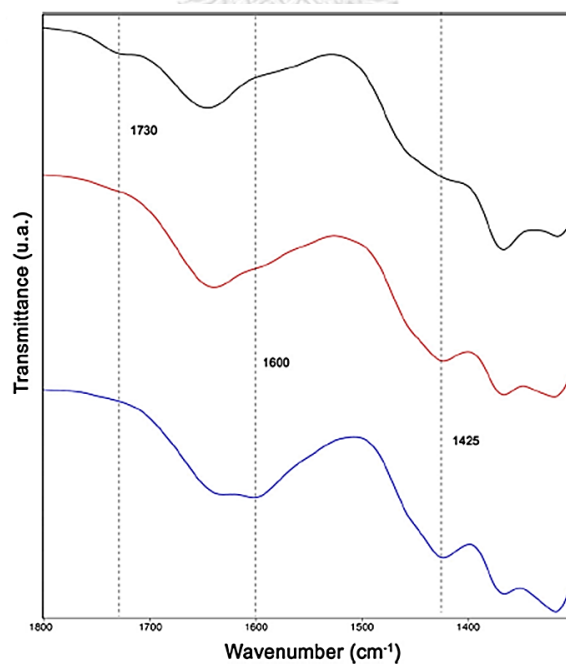


Figure 3.1 FTIR spectrum of BEP, BEP-NaOH and BEP-TEMPO detailed from 1800 to 1300 cm^{-1} [21].

Furthermore, there was a high intensity peak at 1600 cm^{-1} in BEP-TEMPO, which corresponded the symmetric stretching of carboxylate ions. This oxidative treatment (TEMPO) acted in the selective conversion of C6 primary hydroxyl groups of cellulose into sodium carboxylate ones. Thus, the successful oxidation of cellulose nanofibers was confirmed by the observed peak at 1600 cm^{-1} . Figure 3.2 illustrates the width in range of nanometers for untreated and modified (NaOH and TEMPO), respectively. The results suggested that the untreated and chemically pretreated pulps were successfully defibrillated. Moreover, the observed nanofibers presented a web-like structure and most fibers in an entangled conformation for untreated pulp and BEP-NaOH. For the BEP-TEMPO, fibers were separated more finely than the other two examples. Since, the introduction of charged groups during TEMPO-oxidation resulted in nanofibers repulsion, thus improving proper individualization of nano fibers. Figure 3.3 presents that the mechanical properties of nanopapers were enhanced after chemical pretreatment. Particularly, BEP-TEMPO greatly improved the mechanical properties of nanocellulose without increasing the energy demand for defibrillation. BEP-TEMPO presented as the most energy-efficient method in Table 3.1.

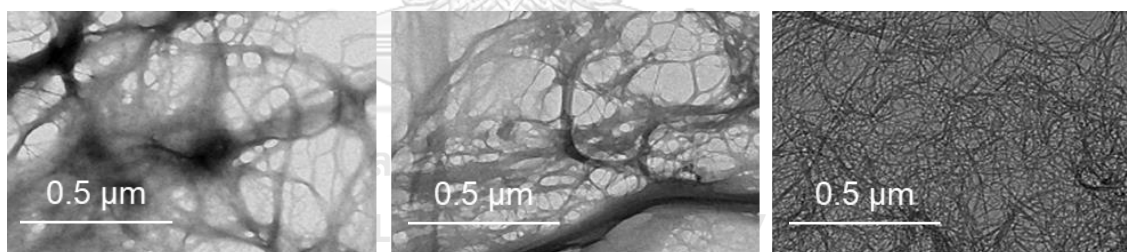


Figure 3.2 Transmission electron micrographs of BEP (a), BEP-NaOH (b) and BEP-TEMPO (c) [21].

Table 3.1 Energy consumption of BEP, BEP-NaOH and BEP-TEMPO [21]

Sample	Energy consumption (kWh/kg)		
	Pretreatment	Grinding	Total
BEP	-	3.8 ± 0.1	3.8 ± 0.1
BEP-NaOH	0.7 ± 0.1	3.7 ± 0.04	4.4 ± 0.04
BEP-TEMPO	0.5 ± 0.04	3.1 ± 0.1	3.6 ± 0.1

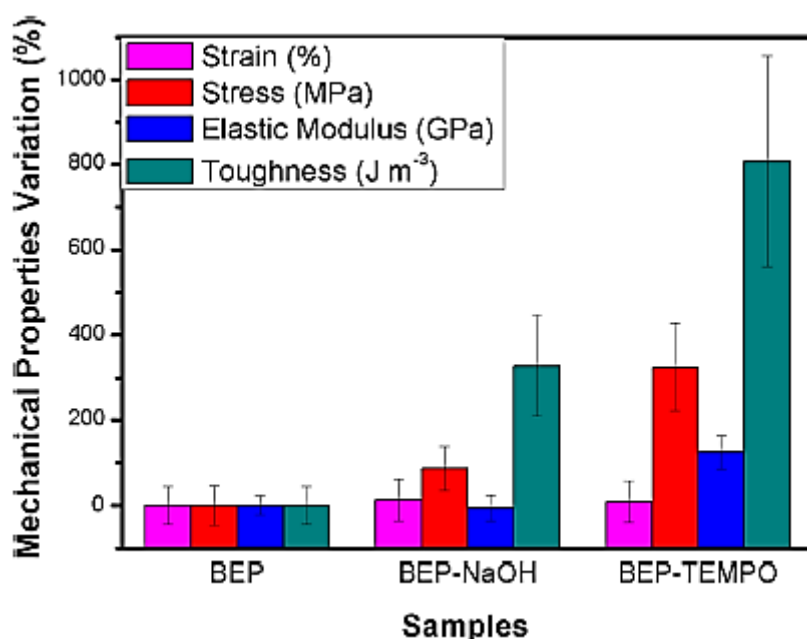


Figure 3. 3 Mechanical properties variation (%) of BEP, BEP-NaOH and BEP-TEMPO [21].

Huang *et al.* (2016) [4] reported about rapid dissolution of spruce cellulose in H₂SO₄ aqueous solution at low temperature. They dissolved a spruce cellulose in 64 wt% H₂SO₄ aqueous solution at low temperature for 2 min, and found that the cellulose solution could form regenerated films with good mechanical properties and transparency. Figure 3.4 presents the FT-IR spectra of cellulose before and after dissolution in H₂SO₄ aqueous solution at -20°C. The absorption peak at 1430 cm⁻¹ (corresponding to the whiskers of cellulose crystalline I) in spruce cellulose weakened and shifted to a lower wavenumber of 1424 cm⁻¹ (corresponding to the cellulose II polymorph) after dissolution and regeneration due to the rotational isomeric in the C3 and C6 hydroxyl groups (rotation around the C3–O3 and C6–O6 bonds). It was explained that the cellulose I crystals had been changed to the cellulose II form after the dissolution and regeneration processes. Moreover, compared to the original spruce cellulose, the band of the O–H vibration of regenerated cellulose shifted to a higher wavenumber (3427 cm⁻¹) and became sharper, which indicated that the hydrogen bonds divide to some extents due to dissolution of cellulose.

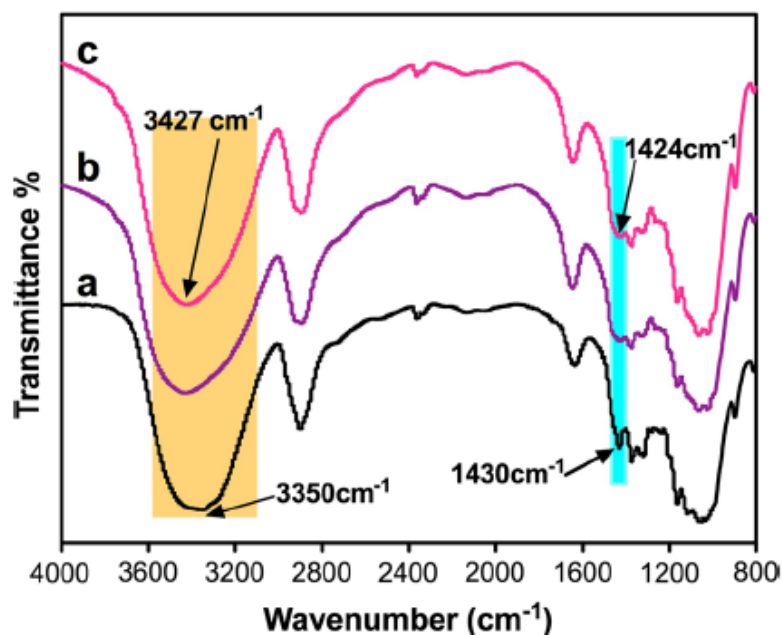


Figure 3. 4 Fourier transform infrared spectra (FT-IR) of spruce cellulose (a), regenerated spruce cellulose made from spruce cellulose/64 wt% H₂SO₄ aqueous solution within 0 (RC-0 min) (b) and 60 min (RC-60 min) (c) [4].

In general, the mechanical properties of regenerated cellulose films depend on molecular weight of cellulose. As shown in Figure 3.5, the molecular weight of cellulose only decreased slightly within 60 min. Therefore, the mechanical properties of regenerated cellulose films were not altered during the storage for 60 min. Furthermore, this research has not only provided the new proof of cellulose dissolution which facilitated the development of cellulose solvent, but also suggested a suitable method to transfer cellulose with high molecular weight into good strength and transparency materials without structure modifications (in Figure 3.6).

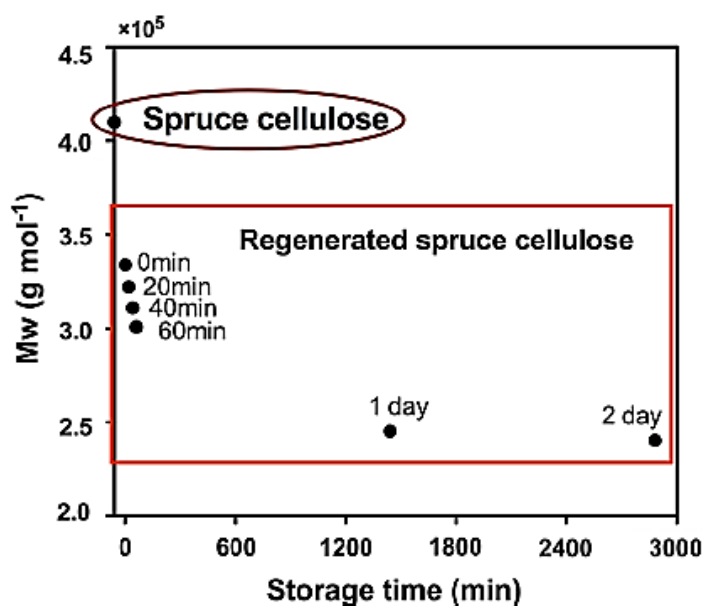


Figure 3.5 Stability of spruce cellulose/64 wt% H₂SO₄ aqueous solution at -20°C: weight-average molecular weight (Mw) of regenerated spruce cellulose made from spruce cellulose/64 wt% H₂SO₄ aqueous solution at different time [4].

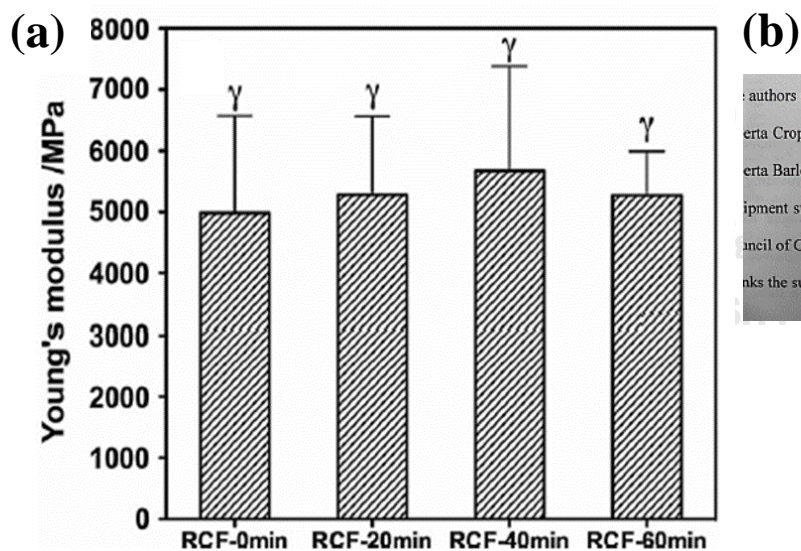


Figure 3.6 Photographs of the transparent regenerated spruce cellulose film (a), and Young's modulus of the regenerated spruce cellulose film for different time (0, 20, 40, 60 min) (b) [4].

Espinosa *et al.* (2013) [22] investigated about isolation of thermally stable cellulose nanocrystals (CNCs) by phosphoric acid hydrolysis. They compared a thermal stability of CNCs obtained by phosphoric acid hydrolysis (P-CNCs) to the CNCs obtained by sulfuric and hydrochloric acid hydrolysis (S-CNCs and H-CNCs, respectively). It was found the P-CNCs exhibited a high thermal stability and formed more stable dispersions in polar solvents such as water, DMSO, and DMF hydrochloric. Figure 3.7 depicted the P-CNCs and H-CNCs turned to yellow at 160°C. In comparison to the S-CNCs, the coloration was less pronounced, even at temperatures of up to 240 °C. Figure 3.8 presents that the H-CNCs had the highest thermal stability. These H-CNCs started to decompose at 220 °C (T_{onset}). Thermal degradation temperature at 5% weight loss (T_{d5}) and the maximum decomposition temperature (T_{max}) were 305 and 350 °C, respectively. The thermal properties of P-CNCs were also similar and had only a minor reduction. The T_{onset} , T_{d5} , and T_{max} of P-CNCs were 220, 290, and 325°C, respectively that were 15–25 °C lower than H-CNCs. Furthermore, the P-CNCs and H-CNCs had a low char yield at 500°C were 6.3 and 12.2%, respectively. However, H-CNCs were difficult to be dispersed in solvents or polymers. Consequently, P-CNCs can be an alternative for multiple applications due to higher thermal stability and more stable dispersions in polar solvents. As shown in Figure 3.9, the dispersions of P-CNCs in H₂O, DMSO, and DMF were found to be stable up to 2 months, whereas dispersions of H-CNCs in those three solvents and dispersions of S-CNCs in DMSO had phase separation after 10 days.

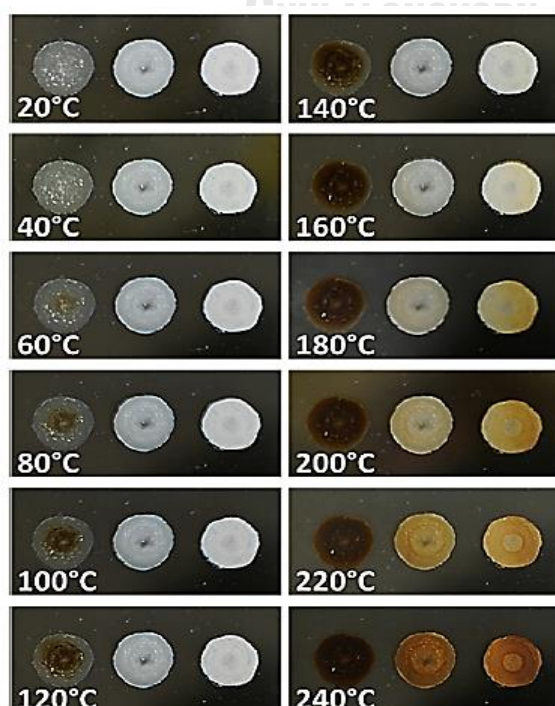


Figure 3.7 Pictures of solution-cast samples of S-CNCs (left), P-CNCs (middle), and H-CNCs (right) heated at a rate of $\approx 7^\circ\text{C}/\text{min}$ [22].

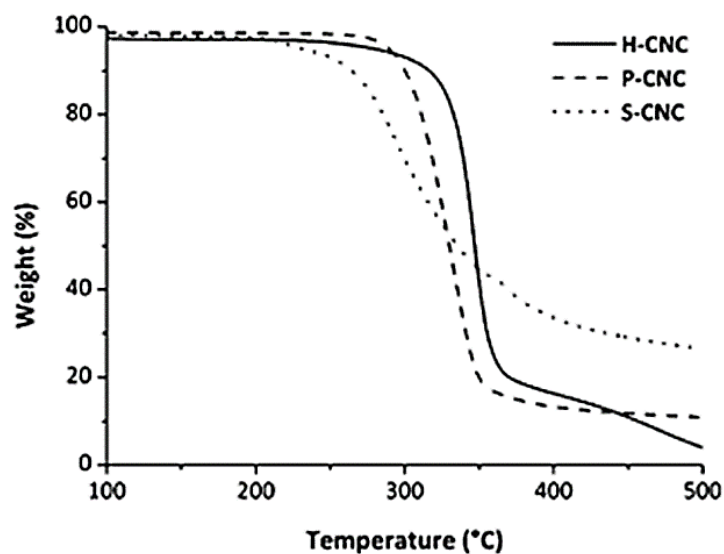


Figure 3.8 TGA thermograms of H-CNCs, P-CNCs, and P-CNCs at the heating rate of 10 °C/min, under air [22].

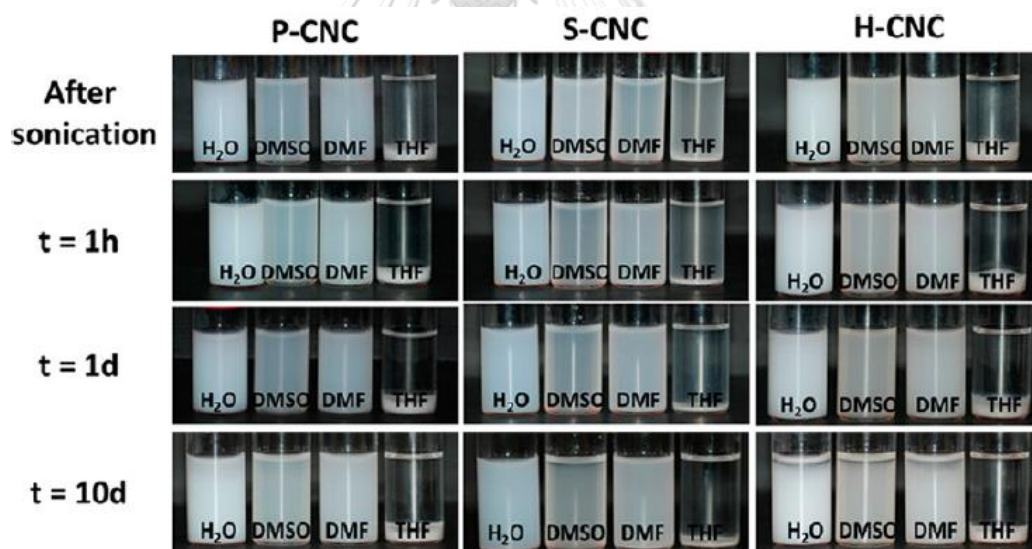


Figure 3.9 Photographs of dispersions of P-CNC, S-CNC, and HCNC in H₂O, DMSO, DMF, and THF (from left to right). In all cases, the CNC concentration was 9 mg/mL, and the dispersion was made by ultrasonication for 10 min. Pictures were taken immediately after preparation, 1 h after preparation, 1 day after preparation, and 10 days after preparation [22].

Jia et al. (2013) [23] reported about preparation and characterization of cellulose regenerated from phosphoric acid. They dissolved the original MCC powder 0.2 g in 85 wt% H₃PO₄ aqueous solution 10 ml at different temperatures. It was found that the reaction temperature was a significant factor in the dissolution of cellulose, as shown in Figure 3.10, the %transmittance of the cellulose solution decreased with increasing temperature. Furthermore, the solubility time did not improve the dissolution of fiber (inset of Figure 3.10). Therefore, a condition at 5 °C for 30 min was chosen for preparing the regenerated cellulose.

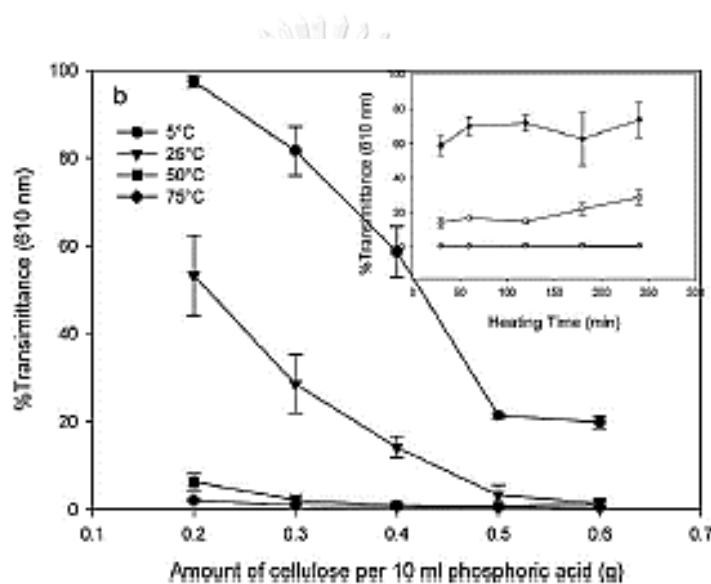


Figure 3.10 effects of ratios of MCC/phosphoric acid, incubation temperature, and time (inset) [23].

They observed five peaks at $2\theta = 14.8^\circ$, 16.5° , 20.5° , 22.7° , and 34.6° for the original MCC, which corresponded to the $(\bar{1}10)$, (110) , (012) , (200) , and (004) crystallographic planes of cellulose I, respectively. Compared with the original MCC, the crystallinity decreased for the regenerated cellulose at $2\theta = 12.3^\circ$ and 20.3° , as shown in Figure 3.11a., which corresponded to the $(\bar{1}10)$ and (110) crystallographic planes of cellulose II. Moreover, the crystallinity index (CI) of the regenerated cellulose was significantly less than that of the original MCC. For the FT-IR spectrum, the absence of peak at 1430 cm^{-1} was observed, which represented to the CH₂ scissoring motion after regeneration. Additionally, The relative peak intensity at

895 cm^{-1} was increased, as shown in Figure 3.11b., which corresponded to the C–O–C asymmetric stretching, [24]. The band at 1430 cm^{-1} was assigned as the crystalline absorption band and was more intensive in cellulose I; the band at 895 cm^{-1} was assigned as the amorphous absorption band and was more intensive in cellulose II and amorphous cellulose [25, 26]. Combining the XRD and FTIR results, the dissolution process could be drawn to firm conclusion that the cellulose lost its crystallinity by the scheme in Figure 3.12.

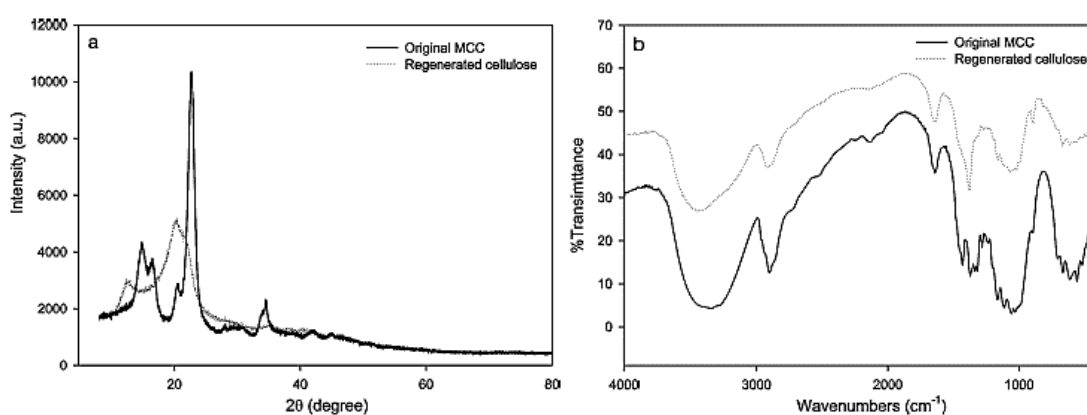


Figure 3.11 XRD (a) and FTIR spectra (b) of original MCC and regenerated cellulose [23].

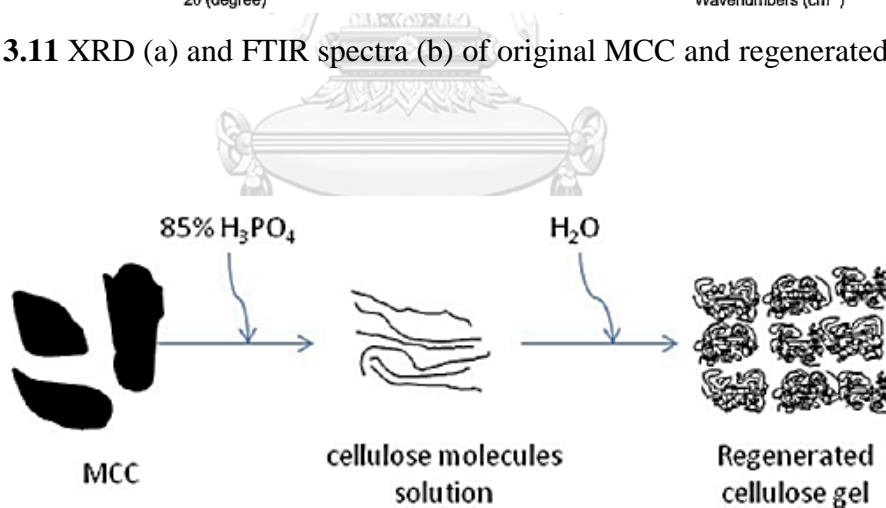


Figure 3.12 Schematic representation of gel formation mechanism of regenerated cellulose [23].

Ngoensawat. et al. (2021) [27] proposed about luminescent nanohybrid of ZnO quantum dot (ZnO QD) and cellulose nanocrystal as anti-counterfeiting ink. The APTES modified ZnO QD (a-ZnO QD) was synthesized as follows: 1.0 mL of KOH (0.5 M in ethanol) was continuously dropped into 10 mL of $\text{Zn}(\text{CH}_3\text{COO})_2$ solution (0.05 M in ethanol) under vigorous stirring. The solution was kept continuously mixing at room temperature for 1 h. The obtained-ZnO QD was modified on the surface by adding a capping reagent (50 mM APTES) in a 1:10 volume ratio to the synthesized ZnO colloid. The mixture was stirred at room temperature overnight to achieve completion of the functionalization process. Figure. 3.13 presents the schematic diagram for the fabrication process of the luminescent a-ZnO QD/BCNC nanohybrid.

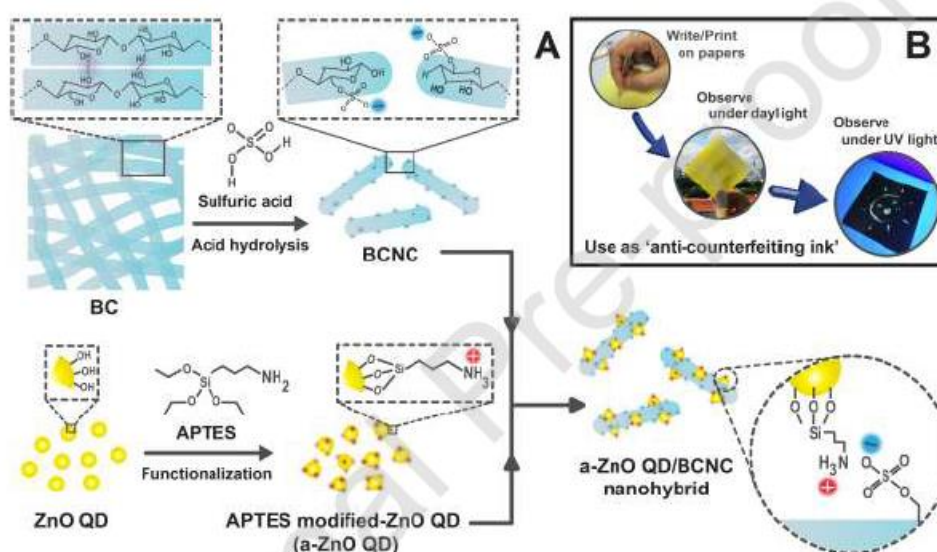


Figure 3.13 (A) Schematic diagram of fabrication method for a-ZnO QD/BCNC nanohybrid *via* electrostatic self-assembly. (B) A use of a-ZnO QD/BCNC nanohybrid suspension as anti-counterfeiting ink [27].

Awan. et al. (2018) [28] investigated about cellulose nanocrystal–ZnO nanohybrids for controlling photocatalytic activity and UV protection in cosmetic formulation. They developed the cellulose nanocrystal–ZnO nanohybrids by using a melamine-formaldehyde (MF)-coated CNC template that provided a mesoporous and nitrogen-rich substrate for the chelated growth of ZnO NPs in aqueous solution. Some insight into the chemical functionalities of the nanocomposite is shown in figure 3.14. For the zinc oxide is normally recognized in the IR spectrum by the characteristic Zn–O stretching vibration between 430 and 500 cm^{-1} , and broad peaks in the range of 3800 – 3900 cm^{-1} indicated to adsorbed water molecules present on the lattice [29]. For comparison, the IR spectrum of the MFCNC–ZnO hybrid shows a distinct absorption at 428 cm^{-1} , which confirms the presence of ZnO in the nanocomposite

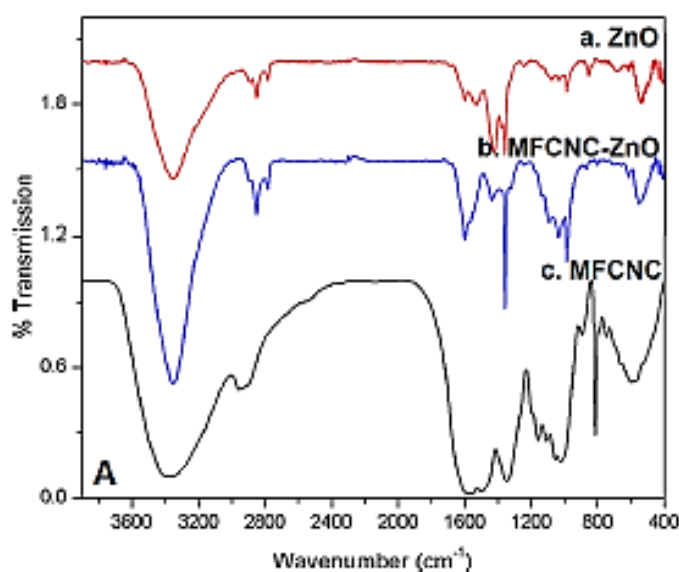


Figure 3.14 FTIR spectra of ZnO, ZNO@MFCNC, and MFCNC measured between 4000 and 400 cm^{-1} [28].

CHAPTER IV

EXPERIMENTAL

4.1 Raw materials

Bleached eucalyptus cellulose pulp was provided by The Siam Cement Group Co., Ltd. (Bangkok, Thailand) and phosphoric acid 85% was obtained from Krungthepchemi Co., Ltd.

4.2 Preparation of regenerated cellulose

Regenerated cellulose was prepared by dissolution of bleached eucalyptus cellulose pulp with 85% H_3PO_4 at $-20^\circ C$. The solution was stirred in ice bath for 0, 20, 40, 60 min, 1 day and 2 days. The regenerated cellulose is coded as RC-0 min, RC-20 min, RC-40 min, RC-60 min, RC-1 day and RC-2 days.

4.3 Preparation of cellulose nanopaper

Cellulose nanopaper was prepared by dry process. The regenerated cellulose suspension was dried in air $25^\circ C$ for 3 days. The cellulose nanopaper is coded as RCNP-0 min, RCNP-20 min, RCNP-40 min, RCNP-60 min, RCNP-1 day, and RCNP-2 days.

4.4 Characterization method

4.4.1 Optical microscopy (OM)

The change in the dissolution process of cellulose nanopaper was observed by a Zeiss optical microscope consisting of 20X interchangeable of objective lens.

4.4.2 Fourier transform infrared (FT-IR) spectroscopy

The chemical structure of cellulose nanopaper were studied by a Nicolet iS5 FT-IR Spectrometer with iD7 ATR accessory (Thermo Fisher Scientific Inc., Waltham, MA, USA). All spectra were taken as a function of time with 64 scans at a resolution of 4 cm^{-1} and wavenumber ranging from $4000\text{-}400\text{ cm}^{-1}$, in transmission mode.

4.4.3 X-ray diffraction (XRD)

X-ray diffraction (XRD) patterns of the cellulose nanopapers were recorded on a diffractometer (model: D/Max-2200, Rigaku) using filtered Cu K α radiation at 40 kV and 20 mA. The scattered radiation was detected in the angular range of 10-40° (2 Θ), with a scanning speed of 2° min⁻¹ (2 Θ) and a step of 0.06° (2 Θ).

4.4.4 Thermogravimetric analysis (TGA)

Thermal stability of cellulose nanopaper were analyzed by thermogravimetric analyzer (model TGA1 Module) from Mettler-Toledo (Thailand). The samples were tested with heating rate of 10 °C/min from 25 to 600 °C under nitrogen atmosphere with a constant N₂ purge gas flow rate of 50 ml/min.

4.4.5 Universal testing machine

Tensile test of the cellulose nanopaper was performed by using an universal testing machine (Instron 5966). Cellulose nanopaper specimens were cut to the dimension of 70 x 10 x 0.02 mm (length x width x thickness) according to standard ASTM D882. At least five replicate samples were tested by using a tension mode at a speed of 12.5 mm/min.

4.4.6 UV-visible spectroscopy

UV-shielding performance of the cellulose/ZnO nanopaper was measured by using GENESYS 10S UV-Vis spectrometer in 300 - 800 nm range.

4.5 Objectives

1. To prepare cellulose nanopaper from regenerated cellulose based on bleached eucalyptus pulp.
2. To analyze properties of cellulose nanopaper including chemical structure, thermal stability, and mechanical properties.

4.6 Scopes of research

1. Preparation of regenerated cellulose by dissolution of bleached eucalyptus pulp
2. Preparation of cellulose nanopaper from dried regenerated cellulose.
3. Investigation of chemical structure of regenerated cellulose by Fourier transform infrared spectroscopy (FTIR).

4. Investigation of thermal stability and mechanical properties of cellulose nanopaper by Thermogravimetric analysis (TGA) and Universal testing machine (Instron 5966), respectively.

4.7 Procedure of the study

1. Reviewing related literature.
2. Preparation of chemicals and equipment for use in this research.
3. Preparation of regenerated cellulose by dissolution of bleached eucalyptus pulp with 85% H_3PO_4 at -20°C . The solution was stirred in ice bath for 20, 40, 60 min, 1 day and 2 days.
4. Preparation of cellulose nanopaper by drying the regenerated cellulose suspension in air 25°C for 3 days.
5. Analysis of chemical structure, thermal stability, and mechanical properties as follows:
 - 5.1 Thermal stability
 - Thermal degradation temperature at 5% weight loss (T_{d5})
 - Char yields at 600°C
 - 5.2 Mechanical properties
 - The tensile strength
 - Elongation at break
6. Analysis of the experimental results.
7. Preparation of the final report.

CHAPTER V

RESULTS AND DISCUSSION

5.1 Eucalyptus cellulose dissolution in H_3PO_4 aqueous solution at low temperature

Figure 5.1 A shows the original bleached eucalyptus pulp (original BEP). After being subjected to mechanical stirring for 5 min, original BEP was added into 98 mL 85 wt% H_3PO_4 aqueous solution pre-cooled to $-20\text{ }^\circ\text{C}$ (Fig. 5.1 B). A transparent cellulose solution was obtained after dissolving in phosphoric acid for 5 min (Fig. 5.1 C3). This obtained transparent cellulose solution was then stored at $-20\text{ }^\circ\text{C}$ for 0, 20, 40, 60 min, 1 day, and 2 days. Figure 5.2 shows the optical microscopic images of eucalyptus cellulose fibers before (Fig. 5.2 A) and after applying mechanical stirring (Fig. 5.2 B). The obtained transparent cellulose solutions are shown in Fig. 5.2 C-F.

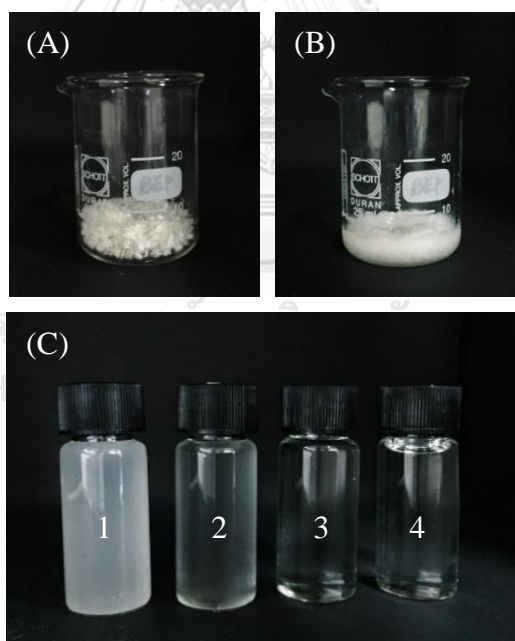


Figure 5.1 images of original BEP (A), BEP in phosphoric acid (B), and cellulose solution after dissolved in phosphoric acid for 2 min (C1), 3 min (C2), 5 min (C3), and 7 min (C4).

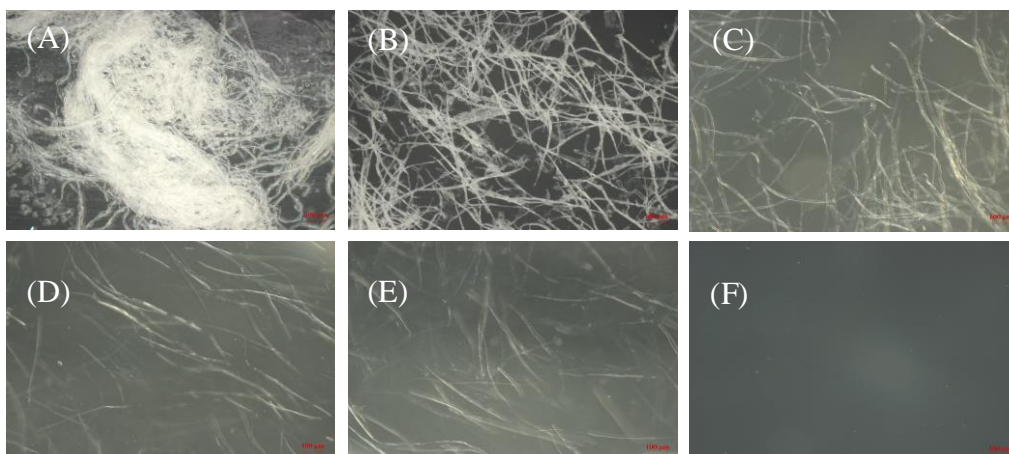


Figure 5.2 optical microscopic images of origin BEP (A), BEP after applying mechanical stirring for 5 min (B), and cellulose solution at 0 min (C), 20 min (D), 40 min (E) and 60 min (F) of storage time.

5.2. Eucalyptus cellulose structure

The FTIR analysis of original BEP and commercial microcrystalline cellulose (Avicel), shown in Figure. 5.3, clearly demonstrate that both spectra have similar absorption bands indicating that no chemical residue is detected in the case of original BEP. The transparent cellulose solution at different storage time were solution casted and dried to form thin film (RCNP). Figure 5.4 (A) shows the FT-IR spectra of original BEP and RCNP at different storage time. It was worth noting that some minor differences existed between the spectra of original BEP and RCNP at different storage time. For the original BEP, the absorption peak at 1427 cm^{-1} (corresponding to the whiskers of cellulose crystalline I) weakened and shifted to a lower wavenumber of 1424 cm^{-1} (corresponding to the cellulose II) in the RCNP spectrum, as shown Fig. 5.4 (B)., due to the rotational isomeric in the C3 and C6 hydroxyl groups (rotation around the C3–O3 and C6–O6 bonds) [30]. In addition, the main broad band in the region of $3500\text{--}3300\text{ cm}^{-1}$ (corresponds to the stretching vibration of OH groups) was observed in the RCNP spectrum. One can also see the appearance of two small peaks in the region of $1231\text{--}1262\text{ cm}^{-1}$ and at 994 cm^{-1} in the RCNP spectrum (Fig. 5.4 C), which could be assigned to P–O and P–OH stretching, confirming the phosphorylation [31].

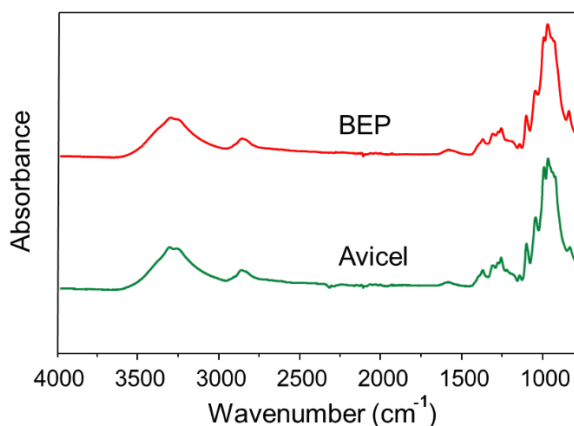


Figure 5.3 FT-IR spectra of original BEP (red line) and Avicel (green line).

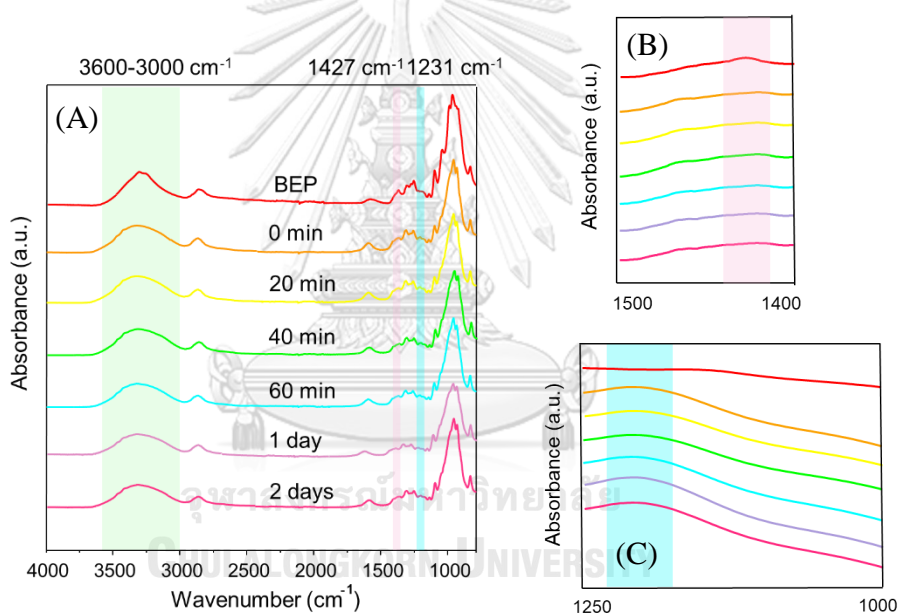


Figure 5.4 FT-IR spectra of original BEP and RCNP at different storage time.

The crystallinity of original BEP and RCNP at different storage time was examined using XRD measurement, and their diffraction patterns are illustrated in Fig. 5.5. The BEP showed the typical diffraction peaks at $2\theta = 15.7^\circ$ and 22.7° , indicating cellulose I type crystal. The RCNP displayed the different peaks at $2\theta = 12.2^\circ$ and 20.6° , which belongs to cellulose II type crystal. This indicated that the cellulose I type crystal transformed to cellulose II type crystal after the dissolution and regeneration [30, 32], and was in good agreement with the FT-IR results. The

crystallinity index (CI) of original BEP and RCNP were calculated from XRD patterns as shown in the inset of Fig. 5.5. The result revealed that the crystallinity index of original BEP decreased after dissolution and regeneration from 47 to 29 %. In addition, the crystallinity index of RCNP was constant at 22% for 60 min of storage time because the inter- and intra-molecular hydrogen bonds and the original crystalline form were broken and reconstructed during the dissolution and regeneration processes [4]. The changes of crystallinity type and index obtained from XRD results agreed well with the optical microscopic images that cellulose fiber could be dissolved completely at 60 min of storage time.

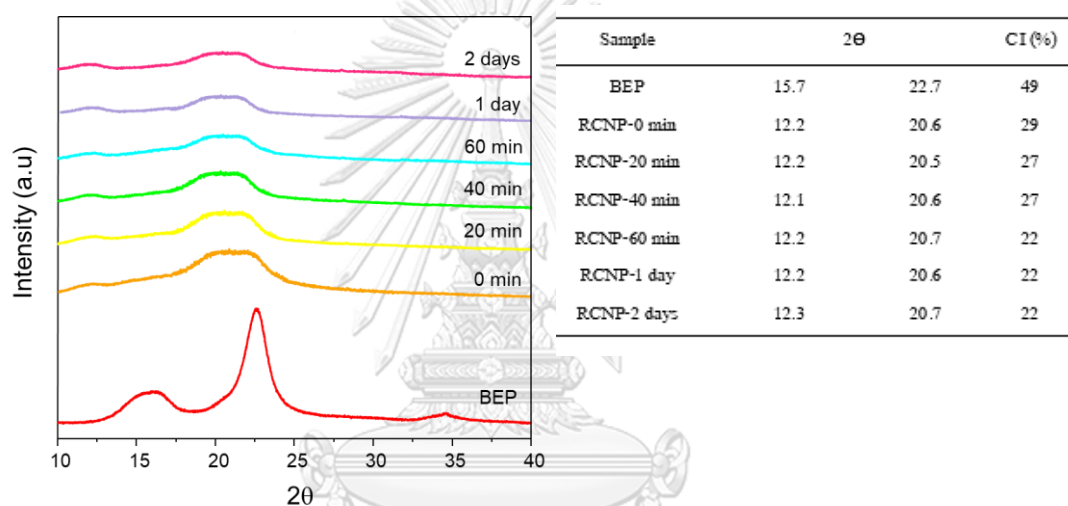


Figure 5.5 XRD patterns of original BEP and RCNP at different storage time.

5.3. Properties of cellulose nanopaper

The thermal stability of the original BEP and RCNP at different storage time were studied using TGA/DTG analysis. The collected TGA/DTG curves of all samples exhibit one thermal degradation step were observed in Figure 5.6. The maximum degradation temperature was decreased from 379 °C to 326 °C for original BEP and RCNP-0 min, respectively. This thermal degradation is associated with the dehydration, decarboxylation, depolymerization and decomposition of glycosylic units in cellulose followed by the char residue formation [33-35]. The thermal stability of RCNP-0 min is slightly reduced in comparison to the original BEP, which is due to the nanometric scale of RC as well as their functionalized surface. At 600 °C, after the main degradation process, the remained char residue is close to 13.6% or 24.9% for original BEP or RCNP-0 min, respectively. The higher char residue

observed in the case of the RCNP in comparison to the original BEP, could be related to the presence of phosphate groups in RCNP, which are well-known for their flame retardant property due to their char forming ability [36].

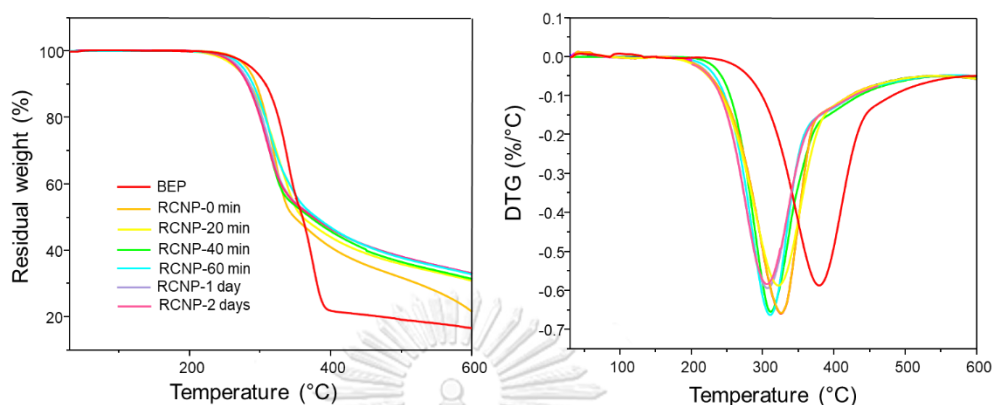


Figure 5.6 TGA and DTG curves of BEP and RCNP at different storage time.

The mechanical properties of RCNP samples are shown in Figure 5.7. The tensile strength and elongation at break increased with increasing the storage time from 22.5 ± 5.7 to 27.0 ± 3.3 MPa and 4.9 ± 1.7 to 5.4 ± 2.3 %, respectively. This is because the higher dissolved cellulose fibers content causing the enlargement of the specific surface area and the aspect ratio of the nanofibers. The specific surface area of nanofibers is larger than that of microfibrils. Therefore, with an increase in the specific surface area and the aspect ratio of the nanofibers, the bonding position of each nanofiber expands and the entanglement of nanofibers in the whole network increases, resulting in higher mechanical properties [37]. Furthermore, the mechanical properties of RCNP after 60 min of storage time were constant due to the complete dissolution of cellulose fibers.

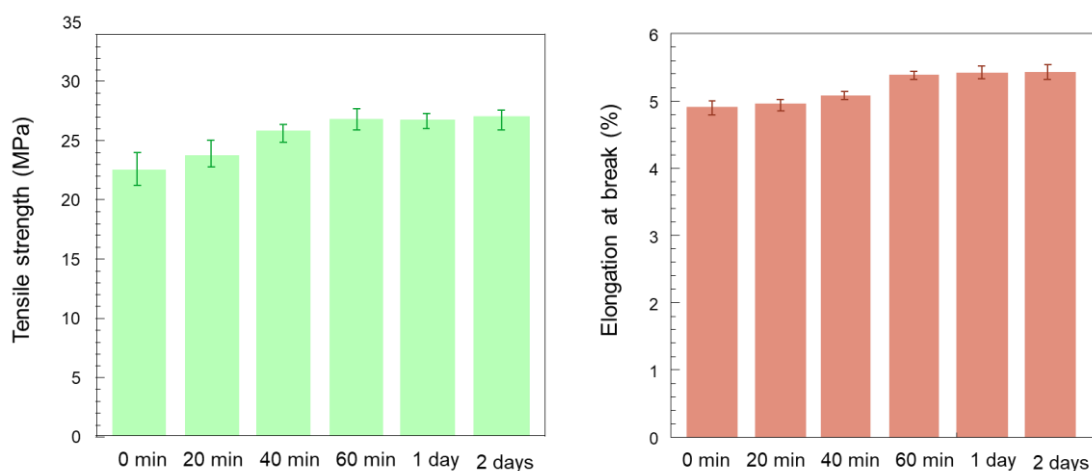


Figure 5.7 Mechanical properties of RCNP at different storage time.

5.4. Molecular comparison of regenerated cellulose nanopaper (RCNP) and nanocrystalline cellulose nanopaper (NCCNP)

The FTIR results were used to verify the transformation from the crystalline to the amorphous structure by the change in two main adsorption bands, as shown in Figure 5.8, where the absorption band at 1429 cm^{-1} and 897 cm^{-1} corresponded to the CH_2 symmetrical bending vibration and the change in molecular conformation from rotation of the β -(1, 4)-D-glucosidic linkage, respectively. The NCCNP was observed to have a sharp absorption at 1429 cm^{-1} and a weak band at 897 cm^{-1} . For RCNP, a broad absorption at 1429 cm^{-1} was observed and the intensity of the absorption at 897 cm^{-1} was higher than NCCNP due to the molecular chains being loosely arranged in amorphous form, unlike the tight compaction in the crystalline form. Therefore, the amorphous structure allowed for more molecular vibration than the crystalline structure [31]. In addition, the intensity of the other bands at 1335 , 1111 , and 1057 cm^{-1} decreased in the case of RCNP. The RCNP also has a higher band absorption at 1648 cm^{-1} which corresponds to the OH bending of adsorbed water due to the free OH group in RCNP. The broad absorption in the $3600\text{--}3000\text{ cm}^{-1}$ region was also observed in RCNP, owing to the OH stretching vibration, which could reflect the changes in hydrogen bonds.

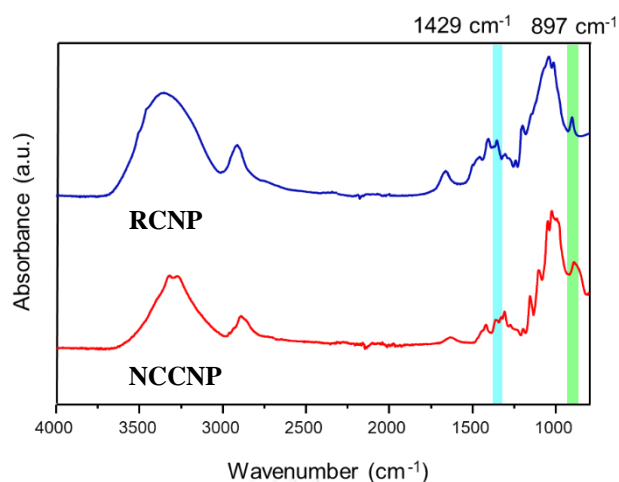


Figure 5.8 FTIR spectra of RCNP and NCCNP.

The TGA curves revealed that the thermal stability of RCNP and NCCNP were very similar, as shown in Figure 5.9. The thermal degradation 10% weight loss temperature (T_{d10}) of RCNP and NCCNP were 256 and 257°C, respectively. Whereas, the char yields of RCNP at 600°C was approximately 21.8% which was higher than NCCNP by about 7%; this was due to amorphous cellulose comprising of cellulose II which was more thermodynamically stable than the other allomorphs [7, 38, 39].

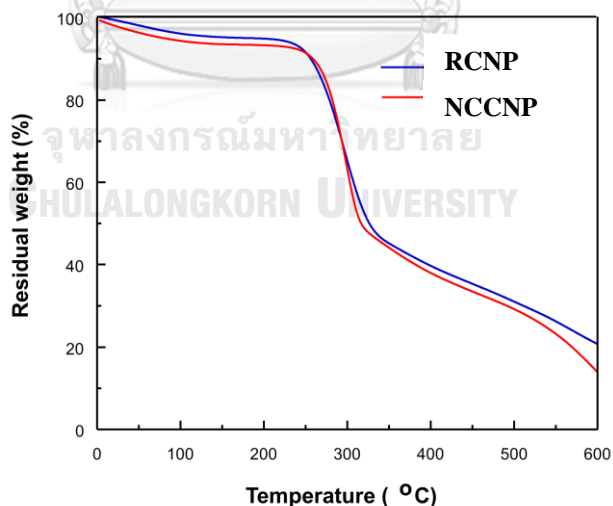


Figure 5.9 TGA curves of RCNP and NCCNP.

The DSC curves of RCNP showed a sharp endothermic peak between 30 and 150°C, as shown in Figure 5.10, which can be attributed to the loss of absorbed water. Meanwhile, the NCCNP indicated broad endothermic peak in the same region, this is

because the crystalline structure is more tightly compacted than their amorphous counterpart leading to a lower amount of absorbed water [31]. The DSC results conformed with the results from FTIR.

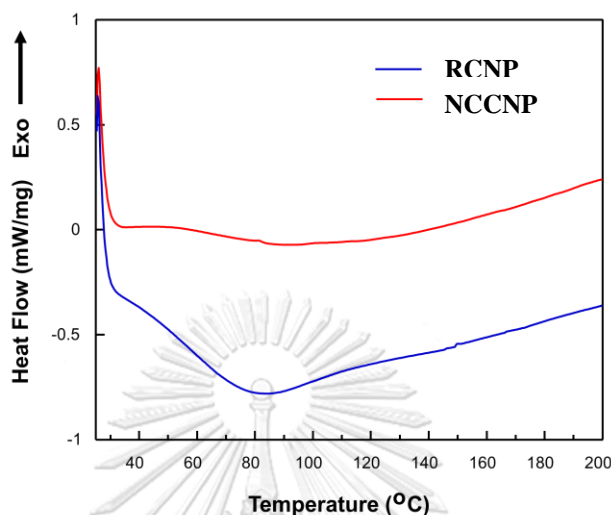


Figure 5.10 DSC curves of RCNP and NCCNP.

Consequently, RCNP can replace NCCNP which was confirmed by the TGA results that the thermal stability of RCNP and NCCNP were very similar. The advantage of RCNP over NCCNP was the low energy consumption required for the fabrication process. In addition, RCNP and NCCNP have the same degree of transparency, thus RCNP can be used in various applications as those of NCCNP with a lower cost of production.

5.5. ZnO nanoparticles embeded on cellulose nanopaper

The FTIR spectra shown in Figure 5.11 offer some insight into the chemical functionalities of the ZnO/cellulose nanopaper. The ZnO nanoparticles is normally recognized in the infrared (IR) spectrum by the characteristic Zn–O stretching vibration between 430 and 500 cm^{-1} [28] and broad peaks in the range of 3800-3900 cm^{-1} attributed to adsorbed H_2O molecules present on the lattice. For comparison, the IR spectrum for the ZnO/cellulose nanopaper shows a distinct absorption at 428 cm^{-1} , which confirms the presence of ZnO nanoparticles in the cellulose nanopaper.

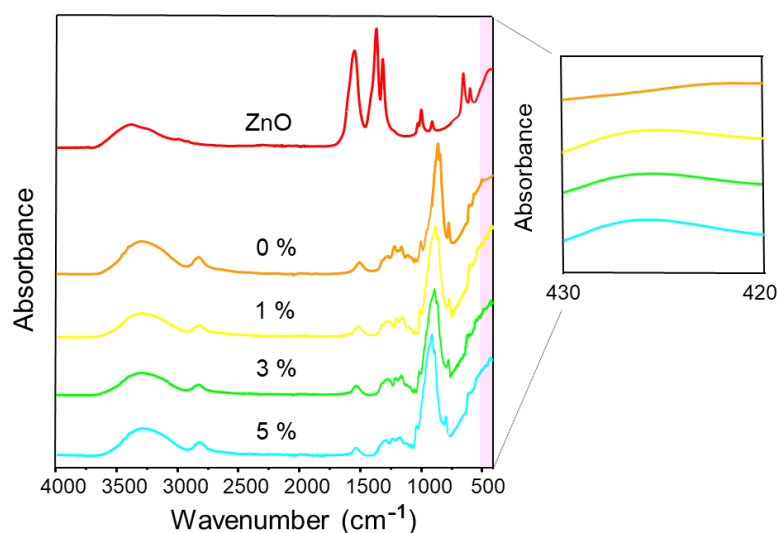


Figure 5.11 FTIR spectra of ZnO nanoparticles and cellulose nanopaper filled with ZnO at contents of 0, 1, 3, and 5 wt%.

The morphology and filler distribution of ZnO nanoparticles in the cellulose nanopaper matrix were examined by scanning electron microscopy (SEM). Figure 5.12 shows the SEM micrographs of pure cellulose nanopaper and cellulose nanopaper filled with ZnO at contents of 1, 3, and 5 wt%. The uniform distribution of ZnO nanoparticles in the cellulose nanopaper matrix at contents of 1 and 3 wt% is shown in Figure 5.12 (B and C). Meanwhile, the excess ZnO content at 5 wt% distributed in the cellulose nanopaper matrix is in the form of filler aggregation as seen in Figure 5.12 (D).

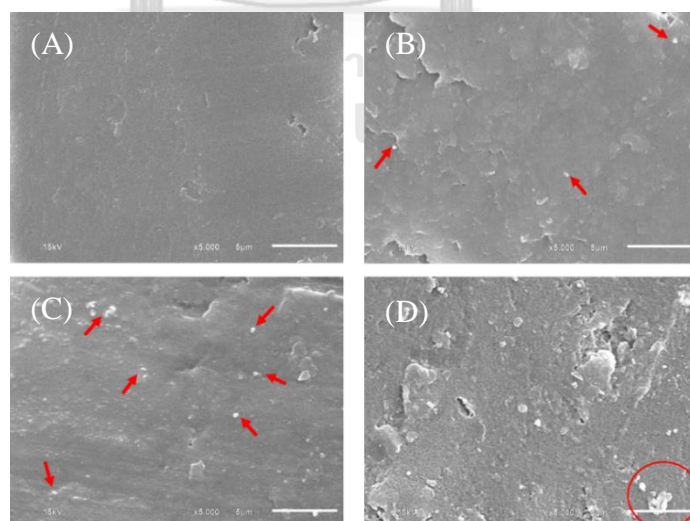


Figure 5.12 Scanning electron micrographs of cellulose nanopaper filled with ZnO nanoparticles at contents of 0 wt% (A), 1 wt% (B), 3 wt% (C), and 5 wt% (D).

The UV-vis transmittance spectra of ZnO/cellulose nanopapers shown in Figure 5.13. It is worth mentioning that the transmittance of the cellulose nanopaper filled with ZnO nanoparticles at contents of 3 and 5 wt% in UV band up from 300 to 380 nm is approximately zero, demonstrating that it blocks UV irradiation in all full UV bands (including UVA and UVB) [40]. In addition, pure cellulose nanopaper and 3 %wt. ZnO/cellulose nanopaper were slight difference degree of transparency. Meanwhile, the 5 %wt. ZnO/cellulose nanopaper had white dots on the cellulose nanopaper due to the ZnO nanoparticles aggregation (as shown in Fig. 5.14). Therefore, cellulose nanopaper embedded with well dispersity ZnO were suggested for its potential optical applications as UV-shielding device.

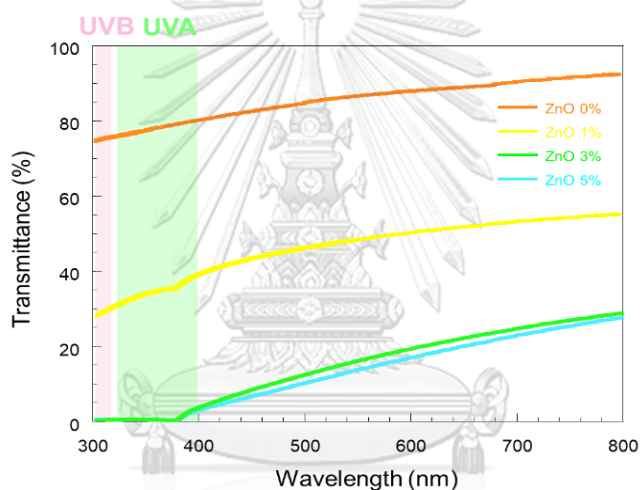


Figure 5.13 Transmission spectra of cellulose nanopaper filled with ZnO nanoparticles at contents of 0, 1, 3, and 5 wt%.



Figure 5.14 images of pure cellulose nanopaper (A) and cellulose nanopaper filled with ZnO nanoparticles at contents of 1 wt% (B), 3 wt% (C), and 5 wt% (D).

CHAPTER VI

CONCLUSIONS

Cellulose nanopaper was successfully fabricated from regenerated cellulose by dissolution BEP in H_3PO_4 aqueous solution with concentration of 85 wt% at low temperature ($-20\text{ }^\circ\text{C}$). FT-IR spectra did not show major changes of eucalyptus cellulose after dissolution and regeneration, while XRD patterns confirmed the transition from cellulose I crystals to cellulose II form with reduced crystallinity index. The optimal storage time for the whole dissolution of cellulose fiber was 60 min. This could be confirmed from optical images and XRD results. The whole dissolution of cellulose fiber affected tensile strength and elongation at break were constant at 26.8 ± 3.4 MPa and 5.4 ± 0.3 , respectively. For the thermal properties of RCNP, char yields at $600\text{ }^\circ\text{C}$ increased from original BEP due to the presence of phosphate groups in RCNP. Lastly, preliminary application of cellulose nanopaper filled ZnO nanoparticles was demonstrated as a UV-blocking film.

REFERENCES



จุฬาลงกรณ์มหาวิทยาลัย
CHULALONGKORN UNIVERSITY

1. Habibi, Y., L.A. Lucia, and O.J. Rojas, *Cellulose nanocrystals: Chemistry, self-assembly, and applications*. Chemical Reviews, 2010. **110**(6): p. 3479-3500.
2. Huang, W., *Chapter 5 - Cellulose Nanopapers*, in *Nanopapers*, W. Huang, Editor. 2018, William Andrew Publishing. p. 121-173.
3. Qi, H., C. Chang, and L. Zhang, *Properties and applications of biodegradable transparent and photoluminescent cellulose films prepared via a green process*. Green Chemistry, 2009. **11**(2): p. 177-18.
4. Huang, W., et al., *Rapid dissolution of spruce cellulose in H₂SO₄ aqueous solution at low temperature*. Cellulose, 2016. **23**(6): p. 3463-3473.
5. Faruk, O., et al., *Biocomposites reinforced with natural fibers: 2000-2010*. Progress in Polymer Science, 2012. **37**(11): p. 1552-1596.
6. Rajinipriya, M., et al., *Importance of Agricultural and Industrial Waste in the Field of Nanocellulose and Recent Industrial Developments of Wood Based Nanocellulose: A Review*. ACS Sustainable Chemistry and Engineering, 2018. **6**(3): p. 2807-2828.
7. Klemm, D., et al., *Cellulose: Fascinating biopolymer and sustainable raw material*. Angewandte Chemie - International Edition, 2005. **44**(22): p. 3358-3393.
8. George, J. and S.N. Sabapathi, *Cellulose nanocrystals: Synthesis, functional properties, and applications*. Nanotechnology, Science and Applications, 2015. **8**: p. 45-54.
9. Atalla, R.H. and D.L. VanderHart, *Native cellulose: A composite of two distinct crystalline forms*. Science, 1984. **223**(4633): p. 283-285.
10. O'Sullivan, A.C., *Cellulose: The structure slowly unravels*. Cellulose, 1997. **4**(3): p. 173-207.
11. Svagan, A.J., M.A.S. Azizi Samir, and L.A. Berglund, *Biomimetic polysaccharide nanocomposites of high cellulose content and high toughness*. Biomacromolecules, 2007. **8**(8): p. 2556-2563.
12. Bhatnagar, A. and M. Sain, *Processing of cellulose nanofiber-reinforced composites*. Journal of Reinforced Plastics and Composites, 2005. **24**(12): p. 1259-1268.
13. Vitz, J., et al., *Extended dissolution studies of cellulose in imidazolium based ionic liquids*. Green Chemistry, 2009. **11**(3): p. 417-42.

14. Zuber, M., et al., *Modification of cellulosic fibers by UV-irradiation. Part II: After treatments effects*. International Journal of Biological Macromolecules, 2012. **51**(5): p. 743-748.
15. From, M., et al., *Tuning the properties of regenerated cellulose: Effects of polarity and water solubility of the coagulation medium*. Carbohydrate Polymers, 2020. **236**.
16. Chang, J.K., et al., *Two-step thermochemical cellulose hydrolysis with partial neutralization for glucose production*. Frontiers in Chemistry, 2018. **6**(APR).
17. Feng, L. and Z.I. Chen, *Research progress on dissolution and functional modification of cellulose in ionic liquids*. Journal of Molecular Liquids, 2008. **142**(1-3): p. 1-5.
18. Sehaqui, H., et al., *Fast preparation procedure for large, flat cellulose and cellulose/inorganic nanopaper structures*. Biomacromolecules, 2010. **11**(9): p. 2195-2198.
19. Wang, J., et al., *Moisture and Oxygen Barrier Properties of Cellulose Nanomaterial-Based Films*. ACS Sustainable Chemistry and Engineering, 2018. **6**(1): p. 49-70.
20. Morales-Narváez, E., et al., *Nanopaper as an Optical Sensing Platform*. ACS Nano, 2015. **9**(7): p. 7296-7305.
21. Malucelli, L.C., et al., *Influence of cellulose chemical pretreatment on energy consumption and viscosity of produced cellulose nanofibers (CNF) and mechanical properties of nanopaper*. Cellulose, 2019. **26**(3): p. 1667-1681.
22. Camarero Espinosa, S., et al., *Isolation of thermally stable cellulose nanocrystals by phosphoric acid hydrolysis*. Biomacromolecules, 2013. **14**(4): p. 1223-1230.
23. Jia, X., et al., *Preparation and characterization of cellulose regenerated from phosphoric acid*. Journal of Agricultural and Food Chemistry, 2013. **61**(50): p. 12405-12414.
24. Oh, S.Y., et al., *FTIR analysis of cellulose treated with sodium hydroxide and carbon dioxide*. Carbohydrate Research, 2005. **340**(3): p. 417-428.
25. Adsul, M., et al., *Facile Approach for the Dispersion of Regenerated Cellulose in Aqueous System in the Form of Nanoparticles*. Biomacromolecules, 2012. **13**(9): p. 2890-2895.
26. Kuo, C.-H. and C.-K. Lee, *Enhancement of enzymatic saccharification of cellulose by cellulose dissolution pretreatments*. Carbohydrate Polymers, 2009. **77**(1): p. 41-46.

27. Ngoensawat, U., et al., *Luminescent nanohybrid of ZnO quantum dot and cellulose nanocrystal as anti-counterfeiting ink*. Carbohydrate Polymers, 2021. **262**: p. 117864.
28. Awan, F., et al., *Cellulose Nanocrystal-ZnO Nanohybrids for Controlling Photocatalytic Activity and UV Protection in Cosmetic Formulation*. ACS Omega, 2018. **3**(10): p. 12403-12411.
29. Jiménez-González, A.E., J.A. Soto Urueta, and R. Suárez-Parra, *Optical and electrical characteristics of aluminum-doped ZnO thin films prepared by solgel technique*. Journal of Crystal Growth, 1998. **192**(3): p. 430-438.
30. Li, R., et al., *Dissolution of cellulose from different sources in an NaOH/urea aqueous system at low temperature*. Cellulose, 2015. **22**(1): p. 339-349.
31. Kokol, V., et al., *Characterisation and properties of homo- and heterogenously phosphorylated nanocellulose*. Carbohydrate Polymers, 2015. **125**: p. 301-313.
32. Zhang, H., et al., *1-allyl-3-methylimidazolium chloride room temperature ionic liquid: A new and powerful nonderivatizing solvent for cellulose*. Macromolecules, 2005. **38**(20): p. 8272-8277.
33. El Achaby, M., et al., *Alfa fibers as viable sustainable source for cellulose nanocrystals extraction: Application for improving the tensile properties of biopolymer nanocomposite films*. Industrial Crops and Products, 2018. **112**: p. 499-510.
34. Collard, F.-X. and J. Blin, *A review on pyrolysis of biomass constituents: Mechanisms and composition of the products obtained from the conversion of cellulose, hemicelluloses and lignin*. Renewable and Sustainable Energy Reviews, 2014. **38**: p. 594-608.
35. Kassem, I., et al., *Phosphoric acid-mediated green preparation of regenerated cellulose spheres and their use for all-cellulose cross-linked superabsorbent hydrogels*. International Journal of Biological Macromolecules, 2020. **162**: p. 136-149.
36. Aoki, D. and Y. Nishio, *Phosphorylated cellulose propionate derivatives as thermoplastic flame resistant/retardant materials: influence of regioselective phosphorylation on their thermal degradation behaviour*. Cellulose, 2010. **17**(5): p. 963-976.

37. Yousefi, H., et al., *Comparative study of paper and nanopaper properties prepared from bacterial cellulose nanofibers and fibers/ground cellulose nanofibers of canola straw*. *Industrial Crops and Products*, 2013. **43**(1): p. 732-737.
38. Fink, H.P., et al., *Structure formation of regenerated cellulose materials from NMMO-solutions*. *Progress in Polymer Science (Oxford)*, 2001. **26**(9): p. 1473-1524.
39. Zhang, B.X., J.I. Azuma, and H. Uyama, *Preparation and characterization of a transparent amorphous cellulose film*. *RSC Advances*, 2015. **5**(4): p. 2900-2907.
40. Li, X., et al., *UV-blocking, transparent and hazy cellulose nanopaper with superior strength based on varied components of poplar mechanical pulp*. *Cellulose*, 2020. **27**(11): p. 6563-6576.



VITA

NAME Nattorn Paijit
DATE OF BIRTH 27 December 1995



จุฬาลงกรณ์มหาวิทยาลัย
CHULALONGKORN UNIVERSITY